1967

Precise measurement of the internal conversion coefficient of the 45-keV transition in U-236

Charles Lewis Duke
Iowa State University

PRECISE MEASUREMENT OF THE INTERNAL CONVERSION COEFFICIENT OF THE 45-KEV TRANSITION IN U-236

by

Charles Lewis Duke

A Dissertation Submitted to the
Graduate Faculty in Partial Fulfillment of
The Requirements for the Degree of
DOCTOR OF PHILOSOPHY

Major Subject: Physics

Approved:

Signature was redacted for privacy.

In Charge of Major Work

Signature was redacted for privacy.

Head of Major Department

Signature was redacted for privacy.

Dean of Graduate College

Iowa State University
Of Science and Technology
Ames, Iowa

1967

TABLE OF CONTENTS

		Page
I.	INTRODUCTION	1
	A. Historical Review	1
	B. Purpose of the Investigation	6
II.	THE THEORY OF THE INTERNAL CONVERSION PROCESS	8
III.	EXPERIMENTAL METHODS	16
IV.	MEASUREMENT BY PHOTON SPECTRUM ANALYSIS	19
	A. The Basic Photon Method	19
	B. The Coincidence Method	24
V.	EXPERIMENTAL INVESTIGATION	30
	A. General Procedure	30
	B. NaI(Tl) Detector and Source Assembly	33
	C. Gating Detector	37
	D. Alpha Spectrum Analysis	38
	E. Efficiency of the NaI(Tl) Detector	44
	F. Response of the NaI(Tl) Detector to Low-Energy Photons	50
	G. Gated Photon Spectrum Analysis	54
	H. Final Results	57
VI.	COMPARISON WITH THEORY	59
VII.	CONCLUSION	63
VIII.	APPENDIX: THE ELIMINATION OF PULSE PILE-UP	64
	A. The Nature of Pile-up	64
	B. The Elimination of Primary Pulse Pile-up	66
	C. Reduction of Pile-up Effects in a NaI(Tl) Pulse Height Spectrum	72

IX. LITERATURE CITED 76

X. ACKNOWLEDGMENTS 81

I. INTRODUCTION

Nuclei in an excited state lose energy by both radiative and non-radiative processes. By far the most probable mode in the radiative channel is the single quantum emission of gamma rays (multiple quantum emission also occurs but so infrequently that it can be completely ignored in this investigation). The two non-radiative processes are internal conversion and internal pair formation. In the experiment reported below, the transition energy is much less than the electron rest mass so that internal conversion processes completely account for the non-radiative channels (pair production is energetically impossible). A measurement of the probability of the internal conversion process for a particular transition is the subject of this study. However, before discussing the nature of the investigation, the internal conversion process will be discussed in detail; from an historical standpoint in the section immediately following, from a theoretical standpoint in the second chapter, and from an experimental viewpoint in the third chapter.

A. Historical Review

In 1910, van Baeyer and Hahn (1) first observed groups of monoenergetic electrons being emitted in the decay of certain radioactive elements. From that time to the present, the internal conversion process has been extremely important in nuclear spectroscopy. In 1922, experiments by Meitner (2) showed that these monoenergetic electrons were not emitted from the nucleus as in beta decay but were ejected from the atomic shells surrounding the nucleus in competition with the emission of nuclear gamma rays. Thus, the energies of the gamma rays could be determined from measurements of the

conversion electron energies and from a knowledge of the electron binding energies. In fact, the measurement of conversion electron energies became the principal method of determining gamma-ray energies until the development of the scintillation counter in 1948.

The term "internal conversion coefficient", defined initially as the probability of electron emission per transition, was first used by Ellis and Wooster (3) in a study of the gamma radiations from RaB (Pb-214). At that time the internal conversion coefficient was thought to be the probability that a gamma ray, after being emitted from the nucleus, would photoelectrically interact with an atomic electron; however, as will be seen later, this conception is incorrect.

After earlier attempts by several groups, Hulme (4) calculated internal conversion coefficients for the K-shell in which the nucleus was assumed to be a radiating electric dipole. His results gave qualitatively good agreement for one group of transitions but not for another group. Mott and Taylor (5) resolved this difficulty by repeating the calculation for the case of a radiating electric quadrupole and reasonable agreement was obtained for this second group of transitions. This was the first use of internal conversion coefficients in the determination of angular momentum changes in nuclear transitions. Finally, magnetic dipole and quadrupole calculations were made by Fisk and Taylor (6) resulting in improved agreement with internal conversion coefficients of other groups of transitions.

Considerable progress was also made during this period in the interpretation of the internal conversion process. Hulme (4), like Ellis and Wooster (3), had assumed that the internal conversion process was the result of the photoelectric absorption of a gamma ray by an atomic electron. However,

Taylor and Mott (7) invalidated this assumption by showing that the observed number of photons emitted per second is equal to the number per second that would be emitted by a bare nucleus (no atomic electrons), with an error of the order of magnitude of the fine structure constant. Thus, de-excitation by gamma-ray emission and by conversion electron emission are two independent, competing processes; the correct interpretation of all previous calculations and measurements is that the internal conversion coefficient should be defined as the ratio of the probabilities of the two decay modes. That is, the meaningful definition of the internal conversion coefficient is the ratio of the rate of electron ejection to the rate of gamma-ray emission (N_e/N_γ) and not the probability of electron ejection per transition $(N_e/(N_e+N_\gamma))$ as thought earlier. Thus, the theory of the internal conversion process was placed on a firm footing by 1933.

The prediction and subsequent discovery of nuclear isomerism (8) indicated that internal conversion coefficients for higher multipoles were needed. Hebb and Uhlenbeck (9) and Dancoff and Morrison (10) then extended Hulme's calculations to include all multipole terms up to angular momentum changes of five, providing a general scheme for classifying transitions and assigning nuclear level properties.

Many problems were associated with these early calculations. The electric multipole internal conversion coefficient calculations were completely nonrelativistic, and the Born approximation was used in the calculation for the magnetic multipoles. In addition, Drell (11) showed that in order to make an accurate calculation, the Dirac 4-component electron theory must be used since ignoring the small components of the electron wave function resulted in serious errors in the magnetic multipole results (the

Pauli 2-component theory had been used in all previous calculations). The development of the scintillation counter[1], which enabled measured and predicted internal conversion coefficients to be compared accurately for the first time, emphasized the need for exact calculations within the framework of relativistic electron dynamics.

Thus, with the advent of high-speed computing devices, Rose and his coworkers began extensive calculations of internal conversion coefficients in which the approximations mentioned above were avoided. The electron wave functions were calculated assuming a point nucleus with a pure Coulomb potential, and the results for the K-shell internal conversion coefficients were tabulated in 1951 (12). At this time calculations which included screening effects were also initiated for the L-subshells. Part of these calculations was published in 1955 (13). However, these calculations, which used more appropriate electron wave functions and performed the numerical integrations to a higher degree of accuracy, added nothing new to the theory of the internal conversion process.

Sliv (14) in 1951 suggested that the finite size of the nucleus could be an important factor, and subsequent calculations (15) for the K- and L-shells showed that the inclusion of the finite size effects resulted in internal conversion coefficients that were significantly different for certain types of transitions than those calculated by Rose, et al. (12,13).

---

[1]With the use of the scintillation counter, the energies and multipolarities of transitions can be experimentally determined.

For example, in magnetic dipole transitions for $Z > 80$, Sliv and Band's values (15) were about 40 percent less than the internal conversion coefficients calculated for a point nucleus. This effect was first verified by Wapstra and Nijgh (16) in a measurement of the K-shell internal conversion coefficient of the 279-keV M1 transition in Tl-203. Rose, following Sliv and Band, included the finite nuclear size in tables published in 1958 (17).

Finally, in 1956, Church and Weneser (18) showed that the expression for the conversion coefficient contains additional matrix elements because of the overlap of the electron wave functions with the nuclear volume. In general, the effect of these matrix elements on the internal conversion coefficient is small, but it can become large when the gamma-ray matrix element is retarded relative to the matrix element for electron ejection. The classic example of this penetration effect is the 1.43 - MeV transition in RaC' (Po-214). This transition, first studied by Gurney (19) in one of the first internal conversion coefficient investigations, is a $0^+ \rightarrow 0^+$ electric monopole transition which occurs only because of nuclear penetration effects (the gamma-ray matrix element is zero, hence gamma-ray emission is forbidden).

One very important consequence of model-dependent nuclear penetration effects is that information regarding nuclear structure may be obtained from internal conversion coefficient measurements for transitions in which these effects are important. However, accurate measurements for transitions in which the nuclear effect is expected to be negligible are necessary in order to establish the reliability of the calculated coefficients. The electric ($2^+ \rightarrow 0^+$) transitions found in a large number of even-even nuclei

represent such a class of transitions. The agreement between experimental and theoretical internal conversion coefficients has been excellent for these transitions except in the deformed nuclei encountered in the rare-earth elements. The first internal conversion coefficient measurements (20) for these nuclei were as much as 20 percent higher than the expected values and led Subba Rao (21) and Bernstein (22) to attempt to correlate these differences with the nuclear deformation parameter. However, by 1965, after many of the measurements had been repeated, no compelling evidence for the existence of anomalous internal conversion coefficients for this region had been found (an excellent review of the experimental results is given in (23)). This question is by no means settled since there are several cases which still do not agree with theory even after internal conversion coefficient measurements have been made using different experimental methods (these measurements confirm each other but are at variance with theoretical values).

B. Purpose of the Investigation

The present investigation is concerned with an E2 transition in a deformed nucleus above A = 226. The nuclear shape in this region is very similar to that in the rare-earth region. Thus, if the E2 internal conversion anomalies described in the previous section are actually a result of the nuclear deformation, it is probable that they are also present or even enhanced for these very heavy nuclei. A knowledge of the internal conversion coefficients for these E2 transitions would be a valuable aid in finding the reason for the existence of the "mysterious" conversion anomalies.

Unfortunately, the very nature of these E2 transitions in the very

heavy nuclei makes the experimental investigation of their internal conversion coefficients difficult. These transitions are characterized by low transition energies (less than 100 keV) and quite large internal conversion coefficients (greater than 100). Thus, the relative gamma-ray intensity is very low which makes an accurate internal conversion coefficient measurement difficult using standard techniques. In fact, with the exception of L-subshell ratio measurements, no internal conversion coefficients for these E2 transitions have been determined with uncertainties less than nine percent.

The purpose of this investigation is to measure accurately (with uncertainty less than five percent) the internal conversion coefficient of the 45 - keV E2 transition in U-236. This nucleus exhibits a non-spherical shape (prolate spheroid) and has a large positive quadrupole moment of $10.35 \pm 0.44 \times 10^{-24}$ cm^2 (24). Thus, a careful measurement of the internal conversion coefficient for this transition between rotational states should help determine the effect of the nuclear deformation on the internal conversion coefficient and hence help determine the range of validity of the most recent internal conversion coefficient calculations (15,17).

II. THE THEORY OF THE INTERNAL CONVERSION PROCESS

Since the actual calculation of internal conversion coefficients is quite a formidable task because of the extensive numerical calculations involved, no explicit calculations will be shown; the results of such efforts are readily available in the various tables (15,17). The purpose of this discussion is to provide a framework within which the theoretical results can be better understood. The various assumptions and methods upon which the calculations are based will be discussed in detail, and a discussion of the results of the calculations will be presented.

Two basic assumptions are made in formulating the theory of internal conversion. The first is the use of perturbation theory in calculating transition probabilities, and the second is that the orbital electron is described by a Dirac one-particle theory. Consider a nucleus, initially in an excited state Ψ_i, and an atomic electron, initially in a bound state ψ_i. Since the nucleus and the electron interact only through the electromagnetic field coupling, a virtual photon can be exchanged between them resulting in a final state Ψ_f for the nucleus and a final continuum state ψ_f for the electron. After summing over the parameters describing the two intermediate states for this second-order process, the resulting matrix element for this transition is (25)

$$M_e = \frac{1}{137} \int d\tau_n \int d\tau_e \, (\vec{J}_n \cdot \vec{J}_e - \rho_n \rho_e) \frac{e^{ik|\vec{r}_n - \vec{r}_e|}}{|\vec{r}_n - \vec{r}_e|} \qquad (1)$$

where the subscripts n and e refer to the nucleus and the electron, respectively. The components of the electron and nuclear four-currents are given by $\vec{J}_e$, $i\rho_e$ and $\vec{J}_n, i\rho_n$, respectively. The transition energy is denoted

by k. All quantities in Equation i are expressed in relativistic units ($\hbar = c = 1$); thus, all lengths and energies are expressed in terms of the electron Compton wavelength and the electron rest mass, respectively. In terms of the Dirac wave functions,

$$\vec{J}_e = \psi_f^* \vec{\alpha} \psi_i \qquad \text{and} \qquad \rho_e = \psi_f^* \psi_i \quad ; \tag{2}$$

however, the explicit form of the nuclear current is dependent upon the use of a particular nuclear model. The matrix element is expanded in the usual multipole expansion and evaluated for various electron states and transition energies. The internal conversion coefficient for a given atomic shell or subshell is proportional to the square of the matrix element, M_e, divided by the square of the matrix element for a gamma-ray emission, M_γ (after summing over the possible final electron states and averaging over the magnetic quantum numbers of the initial system).

This calculation results in an internal conversion coefficient for a transition of a given energy in a given shell. As noted earlier, the internal conversion coefficient, α_i, is the ratio of the rate of electron ejection, $N_e(i)$, to the rate of gamma emission, N_γ;

$$\alpha_i = \frac{N_e(i)}{N_\gamma} \qquad \text{where } i = K, L_I, L_{II}, L_{III}, M_I, \ldots \tag{3}$$

If the subshell internal conversion coefficients for a given shell are summed, the internal conversion coefficient for that shell is obtained. For example,

$$\alpha_L = \alpha_{L_I} + \alpha_{L_{II}} + \alpha_{L_{III}} \quad . \tag{4}$$

Likewise, the total internal conversion coefficient is the sum of the coefficients for all of the electron shells and is denoted by α;

$$\alpha = \alpha_K + \alpha_L + \alpha_M + \ldots \quad . \tag{5}$$

Of course, for α_i to be nonzero, the transition energy must be greater than the electron binding energy for the subshell i.

The internal conversion coefficient is strongly dependent upon the energy of the transition, k. As k decreases, the internal conversion coefficient always increases with the rate of increase being more pronounced at low energies as k approaches the conversion threshold at the electron binding energy. The dependence of the internal conversion coefficient on the atomic number, Z, of the emitting nucleus is not regular; however, the normal behavior is for the internal conversion coefficient to increase with Z. The dependence on the angular momentum transfer is more complicated and will be discussed in detail.

When a transition occurs between final (f) and initial (i) nuclear angular momentum states J_f,π_f and J_i,π_i where J refers to the angular momentum and π refers to the parity, angular momentum L is carried away from the nucleus by either a gamma ray or a conversion electron. The angular momentum transfer, L, must obey the laws of addition of angular momenta and hence can have $2J_s + 1$ values between $|J_f - J_i|$ and $J_f + J_i$ where J_s is the smaller of J_f and J_i. If the parity change, $\pi_i \times \pi_f$, is $(-1)^L$, the transition is said to consist of electric multipole radiation, EL. Likewise, if the parity change is $(-1)^{L+1}$, the transition is composed of magnetic multipole radiation, ML. The internal conversion coefficient is strongly dependent upon the multipole character of the transition because for

different multipoles different non-zero terms enter into the expansion of the matrix element, M_e. The internal conversion coefficients for pure EL and pure ML transitions are designated as $\alpha(EL)$ and $\alpha(ML)$, respectively. Generally, $\alpha(EL)$ and $\alpha(ML)$ differ considerably for all values of L. In fact, this dependence on angular momentum and parity is the reason that internal conversion coefficients have been so important in nuclear physics since their measurement may lead to a unique determination of the multipolarity of the transition.

In general, the internal conversion coefficient is a mixture of the internal conversion coefficients for all the possible L values allowed by the above selection rule, that is

$$\alpha_i = \sum_L \omega_L \alpha_i (L) \qquad \text{where} \qquad \sum_L \omega_L = 1 \quad . \tag{6}$$

The mixing parameters, ω_L, are the relative intensities of gamma rays with angular momentum L emitted in the transition. However, usually only the two terms with the lowest angular momentum contribute (26). For example, with $J_f = 2$ and $J_i = 1$ and no parity change, the multipole field will be an M1 - E2 admixture with

$$\alpha_i = \omega_1 \alpha_i (M1) + \omega_2 \alpha_i (E2) \quad \text{and} \quad \omega_1 + \omega_2 = 1 \quad . \tag{7}$$

If either J_f or J_i is zero (as for example, a transition to the ground state of an even-even nucleus), L is uniquely determined and only one term in the sum is non-zero. Generally, a comparison with theory is easier for this case since no mixing parameters are involved. As mentioned earlier, the two most recent internal conversion coefficient calculations were those by Rose (17) and Sliv and Band (15) (denoted henceforth by R and SB,

respectively). Both calculations resulted in tables of internal conversion coefficients for the K-shell and the three L-subshells. In R, M-shell internal conversion coefficients were also listed for the case of a point nucleus and unscreened electron wave functions. Ten multipolarities were considered, both EL and ML for L equal to one through five. Calculations in R were performed for eight atomic numbers, Z = 25, 35, ..., 95, and for 10 energies from 0.05 to 2.0 mc^2; while those of SB were done at 15 atomic numbers between 33 and 98 and for 18 energies between 0.04 and 5.0 mc^2. The internal conversion coefficients listed at other atomic numbers were obtained by interpolation.

To determine the electron wave functions, the Dirac equation for a single electron moving in a central field was numerically integrated in both R and SB. Screening effects caused by the other atomic electrons were included by using a Thomas-Fermi-Dirac (TFD) potential instead of a pure Coulomb potential outside of the nuclear volume. The effect of screening at low Z was to reduce the K-shell internal conversion coefficients by about 10 percent and the L-shell internal conversion coefficients by up to 40 percent. Finally, the singularity at the origin in the electron wave functions (present with a pure Coulomb potential or pure TFD potential) was eliminated by treating the nucleus as a uniform spherical charge distribution with radius, $R = 1.2A^{1/3} \times (10)^{-13}$ cm. This so-called static effect of nuclear structure is relatively insensitive to the nuclear charge distribution used; that is, once the singularity at the origin has been removed, the resulting internal conversion coefficient is relatively insensitive to the actual shape of the charge distribution. For example, for an M1 transition the static effect reduces the K-shell internal conversion coefficient to about

50 percent of its value in a point nucleus calculation; however, increasing the radius by 10 percent results in only a two percent decrease in the conversion coefficient (27). This effect is even less for other multipoles. The static effect is used only to modify the electron wave functions; all other aspects of the calculation proceed as for a point nucleus. From the above description the same calculations appear to have been performed in both R and SB; however, a major difference arises in the treatment of the dynamical effect of nuclear structure.

The dynamical effect treats the interaction of the electron with the nuclear transition current density within an extended nuclear volume and results in an additional term in M_e that is not present in the matrix element either for a point nucleus calculation or for a calculation including the static effect (27). More specifically, M_e/M_γ is the sum of two terms. The first term, calculated for a point nucleus interaction, is a function of only the electron variables. The second term which includes the interaction over an extended nucleus is dependent upon the details of nuclear structure. The magnitude of this second term (the "penetration matrix element" divided by M_γ) is normally much less than the first term; however, as seen below, this term can have a significant effect on the value of the internal conversion coefficient for certain transitions. The penetration matrix element cannot be evaluated without the use of a specific nuclear model; thus, it is not surprising that the effect is treated differently in R than in SB.

In R, the penetration term was ignored; however, a method to estimate dynamic effects was presented based on specific nuclear models (28). In SB, the simple assumption was made that the nuclear transition current lies on

the spherical nuclear surface in which case an internal conversion coefficient which is independent of nuclear wave functions can be calculated. Note that nuclear deformation effects are not considered by SB. In this "surface current" approximation the penetration terms were found to be only a few percent of the principal term. However, if for a particular transition, the gamma-ray matrix element is hindered while the penetration matrix element is not, this effect can become important. For example, M_γ could be retarded because of a nuclear selection rule which does not affect the penetration matrix element. Both E1 and M1 internal conversion coefficients for transitions of this type have been measured which are 10 to 20 times their tabulated values (29,30). However, in general these effects are expected to be small.

Since the calculations discussed above are very similar, the difference between them is expected to be about two or three percent for the K-shell and about five percent for the L-shell (31), excluding those transitions where the difference in the models is important. However, in a recent study of the two tables (32), systematic discrepancies were found, especially in the internal conversion coefficients for the L-subshells. For example, for low-energy E2 transitions in the L-shell, the differences are quite large and oscillatory at high Z. Dingus and Rud (32) showed that many of these differences can be attributed to a faulty interpolation procedure.

The interpolation procedure used in R was to fit a polynomial of degree seven to the logarithm of the eight calculated points at Z = 25, 35, ..., 95. This procedure is not always satisfactory in the vicinity of the end points Z = 25 and Z = 95 since with a polynomial of degree seven there is little constraint on the shape of the curve in this region. No explanation was

given in SB for the interpolation procedure used in their tables; however, interpolation errors were found normally to be small (32). Thus, in making comparisons of these tables to experimental results accurate to a few percent, care must be taken in using some of the listed internal conversion coefficients. The interpolation procedure used in this investigation will be discussed later. In addition to interpolation errors there are other possible errors in the actual calculations as noted below.

In both R and SB, screening was accounted for by using a TFD potential as explained earlier. However, for certain low-energy transitions, a more realistic screening model is necessary. For example, for the 77-keV M1 transition in Y - 87, Bhalla (33) repeated the calculations using a potential calculated in the Hartree-Fock-Slater approximation. His results differed from R and SB by as much as one percent in the K-shell and as much as nine percent in the L-shell. On the other hand, a recent calculation by Bhalla (34) for low-energy E2 transitions in the rare-earth region using the Hartree model resulted in little or no change in the L-subshell ratios.

Other errors may result from the exclusion of higher-order terms in the perturbation expansion. For example, in the deformed nuclei region, the effect of the nuclear deformation on the electron wave functions for the L_1-subshell may increase the L_1-subshell internal conversion coefficients as much as six percent (34), even though a preliminary calculation in 1958 showed that the effect of nuclear deformation on K-shell internal conversion coefficients was probably quite small (27). Hopefully, the present investigation of the low-energy E2 transition in U-236 will help clarify this problem.

III. EXPERIMENTAL METHODS

Since the internal conversion coefficient is defined as the number of atomic electrons ejected to the number of gamma quanta emitted, a measurement of an internal conversion coefficient usually involves the detection of at least one of these forms of radiation. For the past 50 years, high-resolution magnetic spectrometers have been the basic instrument for observing electron spectra. Today, this instrument is supplemented with the lithium-drifted silicon, Si(Li), detector with which a complete electron spectrum may be recorded in a multichannel analyzer. Since 1950, the principal gamma-ray detector has been the NaI(Tl) crystal. When coupled to a phototube and used with a multichannel analyzer system, this detector has played an extremely important role in practically every area of low-energy nuclear physics. Perhaps just as revolutionary has been the development of the lithium-drifted germanium, Ge(Li), detector with which resolutions have been obtained that are an order of magnitude better than the resolutions obtained with NaI(Tl) spectrometers. With these and other devices many different methods have been developed for the measurement of internal conversion coefficients. However, most of these methods can be grouped into three main divisions: those based on the measurement of electron spectra, the measurement of photon spectra, and the use of coincidence techniques.

Historically, the first method to determine internal conversion coefficients was the detection and analysis of electron spectra. By obtaining the ratio of the area of the appropriate internal conversion peak to the beta continuum which populates the transition, the internal conversion coefficient can be measured (this method is commonly referred to as the peak-to-beta-spectrum method or PBS method). In favorable cases, accuracies

of about three percent can be obtained. The major problem in this type of measurement is that the beta continuum may be distorted in the low-energy region due to beta particles backscattered from the source. Of course, this technique is entirely unsuited for complex decay schemes. One important variation of this method is the internal-external method (IEC method) of Hultberg and Stockendal (35). In experiments of this type, a magnetic electron spectrometer is used to compare the number of internal conversion electrons with the number of electrons ejected by the corresponding gamma rays from an external converter placed near the source. By knowing the absolute photoelectric cross section of the converter along with the angular distribution of the photoelectrons, internal conversion coefficients can be obtained with an accuracy of about five percent. The chief disadvantages of this method are the many parameters that must be determined accurately, such as the converter thickness, photoelectric cross sections, and angular distributions. In fact, a careful calibration with a transition having an accurately known internal conversion coefficient is usually necessary. An advantage of the IEC method is that it can be used with equal precision for complex or simple decay schemes.

Since the ejection of atomic electrons results in the emission of X-rays (with probability determined by the fluorescence yield), the analysis of photon spectra can be used to determine K-shell internal conversion coefficients. By knowing the relative efficiency of the detector for the gamma rays and K X-rays and by knowing the fluorescence yield for the K-shell, internal conversion coefficients for the K-shell can be obtained to an accuracy of about three percent from the relative areas of the K X-ray peak and the gamma-ray peak. A further discussion of this technique will

be presented in the next chapter.

By introducing coincidence techniques, two types of detectors can be combined in a single experiment. For cascading transitions, the normal method is to record electron-gamma coincidences with an electron spectrometer and gamma-ray detector or electron-electron coincidences with beta-ray spectrometers. Of special interest in this area is the coincidence spectrometer, designed by Easterday et al. (36), using semiconductor detectors. Internal conversion coefficients measured with this device have been accurate to only 10 percent; however, as the efficiency calibrations for these detectors are improved, the uncertainties are expected to be much less.

Finally, there are several methods which do not fall into any of the above catagories but which are useful for various types of transitions. The most important of these, as far as this investigation is concerned, is the determination of total internal conversion coefficients from Coulomb excitation and lifetime measurements. From the inelastic-scattering cross section derived from Coulomb excitation, the reduced transition probability, B(E2), can be determined (only E2 transitions are considered here). Since a measurement of the lifetime of the excited level yields the product B(E2) x $(1+\alpha)$, the total conversion coefficient can be determined. The only measurements of total internal conversion coefficients for E2 transitions in the transuranic elements have been made by this method (37); however, the uncertainties are quite large, never less than nine percent.

There are many interesting variations to all of the above methods. For example, by adding a gating detector, the PBS method can be extended to more complex decay schemes. A similar variation that extends the photon spectrum method is discussed in the next chapter.

IV. MEASUREMENT BY PHOTON SPECTRUM ANALYSIS

A. The Basic Photon Method

One of the most accurate methods for the measurement of internal conversion coefficients is the basic photon method. In this method the internal conversion coefficient is determined by a careful analysis of the photon spectrum resulting from the decay of a nuclear excited state. The explicit assumptions must be made that this state is not fed by electron capture; that any particles (alpha, beta, gamma) populating this level, or resulting from other transitions, do not interfere with the photon spectrum; and that no conversion electrons are seen by the photon spectrometer. These assumptions normally restrict the application of this method to nuclei with only one excited state populated in the decay of the parent isotope.

The photon spectrum is recorded by a photon spectrometer which is normally composed of a NaI(Tl) detector, preamplifier, amplifier, and multichannel pulse height analyzer. This spectrometer counts the number of photons detected with an energy between E and $E + \Delta E$ as a function of the energy, E, given to the NaI(Tl) crystal by the photon (ΔE is the channel width of the multichannel analyzer). For energies below 200 keV, all of the photon energy is usually transferred to the crystal. In general, phototube noise and photon absorption by intervening materials between the source and NaI(Tl) crystal place a lower limit of about 10 keV on the photon energy that can be observed. Thus, only K X-rays for $Z > 35$ and L X-rays for $Z > 80$ can be recorded by the spectrometer. Since these X-rays are a direct consequence of internal conversion, their production and detection will be considered in more detail.

If the transition energy is greater than the K-shell binding energy,

internal conversion may occur in the K-shell resulting in the emission of K X-ray groups. Since the energy difference between these X-ray groups is much smaller than the resolution of the NaI(Tl) detector, the resulting K X-ray spectrum will be observed as a single peak. L X-rays can also be emitted as the vacancy, originally in the K-shell, moves outward in accordance with atomic selection rules and as internal conversion occurs in the L-shell[1]. Thus, the presence of L X-rays does not necessarily imply that L-shell internal conversion has occurred. However, if the transition energy is less than the K-shell binding energy but greater than the L-shell binding energy, the only mode of production of L X-rays will be from vacancies created by internal conversion in the L-shell. Since the emission of a gamma ray implies that internal conversion did not occur for that particular transition, the detection of the X-rays and gamma rays can be used as signals which indicate whether internal conversion has or has not occurred. Hence, probability equations can be written which describe the conversion process in terms of the recorded photon spectrum. These equations will be developed for internal conversion in the K-shell; however, they will apply equally well for L-shell internal conversion, provided that internal conversion in the K-shell is forbidden by conservation of energy.

If the number of counts recorded in a specific time in the K X-ray peak and gamma-ray peak is denoted by N_K and N_γ, respectively, the probability equations describing the transition are

---

[1]Lower-energy X-rays such as M, N, and O X-rays are also emitted in the same manner as the L X-rays; however, only the K and L X-rays are included in this discussion.

$$N_K = N_o \frac{\alpha_K}{1+\alpha} \omega_K \epsilon_K \tag{8}$$

and

$$N_\gamma = N_o \frac{1}{1+\alpha} \epsilon_\gamma \tag{9}$$

where N_o is the total number of transitions occurring in the source during the counting time. The detection probabilities for the X-rays and gamma rays are given by ϵ_K and ϵ_γ, respectively. The probability of K X-ray emission following internal conversion in the K-shell is given by the fluorescence yield, ω_K[1]. Finally, from the definition of the internal conversion coefficient, $\alpha_K/(1+\alpha)$ and $1/(1+\alpha)$ are the respective probabilities that either a K-shell conversion electron or a gamma ray will be emitted during a particular transition.

By taking the ratio of Equations 8 and 9, the K-shell internal conversion coefficient is given by the expression;

$$\alpha_K = \frac{1}{\omega_K} \frac{\epsilon_\gamma}{N_\gamma} \frac{N_K}{\epsilon_K} . \tag{10}$$

All of the terms on the right-hand side of this equation can either be calculated or experimentally determined as described in the following paragraphs.

The efficiency, ϵ, is defined as the probability that a photon, after being emitted by the source, will lose part or all of its energy in the NaI(Tl) crystal. With the aid of a Fortran computer program[2], ϵ can be

---

[1]The process competing with X-ray emission is the Auger effect in which radiationless transitions occur with the ejection of an outer atomic electron as the vacancy moves outward.

[2]Ames Laboratory computer program library; Distribution No.: 707409651100100.

accurately calculated. This program is discussed in a following chapter. The result of this calculation shows that for low-energy photons (less than 30 keV), the efficiency decreases with energy as a result of increased absorption by materials between the source and the crystal. Thus, the efficiency is not constant for the various K X-rays, and N_K/ϵ_K in Equation 10 should be replaced by a sum over the K X-ray groups weighed by the reciprocal of the efficiency, i.e. $\sum_i N_K^i/\epsilon_i$. Since L X-rays can have an energy range from about 10 keV for the L_α group to about 20 keV for the L_γ group ($Z > 80$), this effect on the efficiency is particularly noticeable when the basic photon method is applied to L-shell conversion.

The fluorescence yield for the K-shell, ω_K, has been measured for many different elements. The experimental methods are straightforward with vacancies in the K-shell usually being produced by bombarding the atom with protons, electrons, or heavy charged particles of sufficient energy to cause ionization in the K-shell. By knowing the probability of creating a K-shell vacancy and by measuring the intensity of the K X-rays emitted, ω_K can be determined with an accuracy of one percent or less. L-shell fluorescence yields are much more difficult to measure.

The L-shell is composed of eight electrons in three subshells (L_I, L_{II}, L_{III}); thus, a fluorescence yield (ω_I, ω_{II}, ω_{III}) can be defined as before for each of the subshells. However, two problems make the determination of these subshell fluorescence yields difficult. First, the ionization of only one of the L-subshells is difficult experimentally. Usually, all three subshells are ionized in some specific ratio so that a mean fluorescence yield, $\bar{\omega}_L$, is determined which depends on the relative number of vacancies in the three subshells. Second, radiationless transi-

tions can occur between the L-subshells moving a vacancy from one subshell to another ($L_I \rightarrow L_{II}$, $L_{II} \rightarrow L_{III}$, $L_I \rightarrow L_{III}$). These transitions, known as Coster-Kronig transitions[1], can change the original distribution of vacancies in the L-subshells and hence have to be accounted for in any measurement of ω_I, ω_{II}, or ω_{III}. Several measurements of the average fluorescence yield have been made in the heavy elements above A = 226 in which L-shell internal conversion in low-energy E2 transitions was used to create the primary L-shell vacancies (38). Thus, $\bar{\omega}_L$ determined in this manner can be used in the determination of α_L for the same E2 transition because the relative number of primary L-shell vacancies are the same.

The photon intensities, N_K and N_γ, are experimentally determined from the photon spectrum. However, to obtain these intensities, the various mechanisms by which the photons interact with the NaI(Tl) crystal must be well understood. In general, any process or combination of processes that results in the complete absorption of a photon in the crystal gives rise to a Gaussian peak (photopeak) in the photon spectrum whose mean position corresponds to the photon energy. On the other hand, incomplete photon absorption or the absorption of a photon that has been scattered external to the crystal produces a continuous distribution below the photopeak. The main components of this distribution are the escape peak and the Compton distribution. Thus, in determining the intensity of a gamma ray or X-ray, both the number of counts in the photopeak and the number below the photopeak must be determined. In this investigation, a large

---

[1]Coster-Kronig transitions are not to be confused with Auger transitions since Auger transitions are defined as radiationless transitions between major shells, not between the subshells of a major shell.

well-type NaI(Tl) crystal was used for the photon detector. This type of detector simplifies the spectrum analysis considerably since the number of incompletely absorbed photons which give rise to the distribution below the photopeak are drastically reduced (especially if the photon energy is less than 150 keV).

Thus, by means of a relatively simple technique, K-shell internal conversion coefficients may be measured with uncertainties of less than three percent in favorable cases. However, the limitation to one excited state means that the method can be applied in only a very few cases. Furthermore, even if it can be applied, N_o (and hence the total internal conversion coefficient) cannot be determined. Therefore, it is desirable to extend the photon spectrum method so that more complicated decay schemes can be considered and so that N_o can be determined.

B. The Coincidence Method

The coincidence method is closely related to the basic photon method. In the coincidence method the photon spectrum of an isotope is observed in coincidence with a particle (alpha, beta, gamma) populating the nuclear excited level of interest. The transition from this level is assumed to be a ground-state transition not fed by electron capture, with a lifetime of less than 10^{-8} sec. By using this technique where it is possible to gate uniquely on the transition of interest, the total internal conversion coefficient as well as the K-shell internal conversion coefficient may be determined. In addition, fewer assumptions have to be made about the complexity of the decay scheme.

A second particle detector (gating detector) with associated electronics is placed near the source and is used to generate a signal that will acti-

vate the photon spectrometer whenever a particle populating the nuclear excited level is detected (the signal is used to open a gate at the input of an analog-to-digital convertor, ADC, of a multichannel analyzer). Thus, if N_o is redefined to be the observed rather than the total number of transitions, N_o will be equal to the total number of times that the photon spectrometer is activated. In other words, the photon spectrometer will observe only that fraction of the total number of transitions in which particles in coincidence with the transition of interest are detected.

Normally, N_o is determined by counting with a scaler the number of times the ADC gate is opened. However, a dead-time correction must be made because the multichannel analyzer may be busy processing a previous pulse at the time the analyzer gate is opened. One way to avoid this dead-time correction is to use a method devised by Dingus *et al.* (39). In this method, a summing technique is used in which the gating pulses from the gating detector are not only sent to the analyzer gate but are also sent to a linear adding circuit where they act as a pedestal to which the pulses from the NaI(Tl) detector are added before being sent to the multichannel analyzer. Thus, the observed photon spectrum is shifted by the number of channels corresponding to the height of the pedestal pulse, and a pedestal peak is produced in the channel corresponding to zero energy for the photon spectrum[1]. The observed number of transitions, N_o, is now the number of times the ADC gate is opened when the analyzer is

---

[1]The pedestal peak is present because a K X-ray or gamma ray is not detected everytime the ADC gate is opened. In this discussion any lower-energy X-rays in the photon spectrum, such as L X-rays, are assumed to fall into the pedestal peak. Thus, the pedestal peak is composed of a zero-energy peak plus low-energy X-rays. Of course, the K X-ray peak must be adequately resolved from these low-energy X-ray peaks.

able to accept and process a pulse and is given by the total area of the photon spectrum including the pedestal peak. In this simple manner, the problem of dead time has been eliminated.

Since the shapes of the X-ray and gamma-ray peaks in the photon spectrum have not been changed by the addition of the pedestal pulse, the probability equations for N_K and N_γ will have the same form as those developed in the discussion of the basic photon method. Thus, Equations 8 and 9 are also valid for the coincidence method. In particular, an expression for the total internal conversion coefficient can be obtained from Equation 9;

$$\alpha = \epsilon_\gamma \frac{N_o}{N_\gamma} - 1 . \qquad (11)$$

Therefore, from an analysis of the photon spectrum and pedestal peak, α as well as α_K may be determined. The photon intensities, efficiencies, and fluorescence yields are determined in the same manner as discussed in the previous section. However, in order to obtain an accurate measurement of the internal conversion coefficients, several effects associated with the response of the gating detector must be examined in detail.

There are various problems connected with the gating detector. The detector must provide a unique gate for the transition of interest. For example, when gating with gamma rays, the gamma ray populating the nuclear excited level should be the one of highest energy; otherwise, the Compton tails from higher-energy photons will introduce unwanted gating pulses. Likewise in gating with beta particles, the beta group populating the nuclear excited level should be the one of highest energy. The lower-energy beta groups can then be absorbed, or a discriminator can be set above

the end-point energies of the lower-energy groups. When gating with alpha particles using high-resolution semiconductor detectors, tailing from higher-energy alpha groups can also cause the gate to trigger. Since many alpha emitters have an intense high-energy ground-state alpha group, there is no easy solution to this problem, and it will be discussed in the next chapter.

As mentioned earlier, the conversion electrons must be absorbed before reaching the NaI(Tl) detector so that the photon spectrum is not distorted by the summing of electron and gamma responses. Likewise, the detection of conversion electrons in the gating detector can distort the gating spectrum. For example, when gating with alpha or beta particles, the conversion electrons, if allowed to reach the gating detector, can sum with the gating particles and cause the alpha or beta spectrum to be shifted by an amount corresponding to the energy of the conversion electrons. Therefore, some of the gating pulses may be summed above the window set across the gating spectrum. For this reason, the window sees two effective count rates, one when the transition decays by gamma emission (no conversion electrons present) and one when the transition decays by internal conversion (in which case summing is possible). Thus, the gated photon spectrum will be biased in favor of the decay by gamma-ray emission with a resulting error in the measured internal conversion coefficient. To avoid this error when gating with beta particles, the energy of the gating particles should be much larger than the energy of the conversion electrons so that the conversion electrons can be absorbed before reaching the gating detector. When gating with alpha particles, this problem can be minimized by placing the alpha detector as far from the source as possible in order

to decrease the solid angle subtended by the alpha detector relative to the source. If these effects related to the gating detector are minimized, an accurate determination of α and α_K is possible.

As a final note, the coincidence method can be extended to two other cases. If the nuclear level is uniquely populated by electron capture, it is possible to gate on the K X-rays and obtain α and α_K from an analysis of the photon spectrum. Likewise, for two coincident transitions the high probability of summing for a well-type NaI(Tl) detector can be used to determine α and α_K for both of the transitions. The photon spectra and probability equations for these cases are discussed by Dingus et al. (40).

The most important feature of the coincidence method is the high accuracy with which internal conversion coefficients can be measured. Dingus et al. (39) have obtained uncertainties of less than two percent for ground-state E2 transitions in some rare-earth isotopes by gating on gamma rays and beta particles. Aside from the requirement of a multichannel analyzer, the electronics are fairly simple and straightforward (for example, compare to the apparatus of an internal conversion coefficient measurement using a beta-ray spectrometer). On the other hand, the data analysis can become involved since small effects have to be considered, such as iodine K X-ray escape peaks (a feature intimately associated with NaI(Tl) detectors), events that occur below the photopeak due to Compton scattering, accidental summing, bremsstrahlung, and contamination from other transitions. However, no important corrections due to angular correlation effects are necessary (a small correction, easy to determine, is necessary when gating with alpha particles), and the

dead-time problem has been eliminated. With the use of a well-type NaI(Tl) detector, weak sources (0.1 to 0.5 microcuries) can be used so that the creation of K and L X-rays following photoelectric absorption in the source itself will be quite small.

The major disadvantage of this method is the limitation imposed upon the decay scheme in order to make available a unique gate. However, if the method can be applied, it is one of the most accurate ways to determine the total internal conversion coefficient. A measurement of the K-shell internal conversion coefficient is less accurate because the fluorescence yield introduces more uncertainty. In fact in most cases, the K-shell internal conversion coefficient can be determined more accurately by taking the product of the total internal conversion coefficient (measured with the above method) with the K-to-total ratio measured with a beta-ray spectrometer.

V. EXPERIMENTAL INVESTIGATION

From the decay scheme of Pu-240 shown in Fig. 1, it can be seen that the 45-keV transition in U-236 is populated primarily by the 5.115-MeV alpha group (41). Thus, the total internal conversion coefficient of this transition can be measured by an application of the coincidence method in which the 45-keV ground-state transition is uniquely gated by the 5.115-MeV alpha group from the decay of Pu-240.

A. General Procedure

An isotopically pure Pu-240 source was placed at the bottom of the well of a well-type NaI(Tl) crystal optically coupled to a DuMont 6363 phototube. A small, semiconducting alpha detector was inserted into the well and positioned directly above the source. As shown in Fig. 2, pulses from the gating (alpha) detector were sent through a preamplifier (Tennelec TC-130), linear amplifier (Tennelec TC-200), biased amplifier (Tennelec TC-250), into a single channel analyzer (Hamner N-685). The window on the single channel analyzer was set across the 5.115-MeV alpha peak so that an output signified that the 45-keV level had been populated. The output from the single channel analyzer triggered a one-shot multivibrator which generated both a positive and a negative pulse of two microseconds duration. The negative pulse was sent to a linear adder to act as a pedestal for the pulses from the NaI(Tl) detector. The positive pulse was used to open the gate to the ADC of the multichannel analyzer (Nuclear Data ND-180FM). Pulses from the NaI(Tl) detector were sent through a double delay-line amplifier (Hamner N-380) and into the linear amplifier of the multichannel analyzer. Here the pulses were given the proper pulse

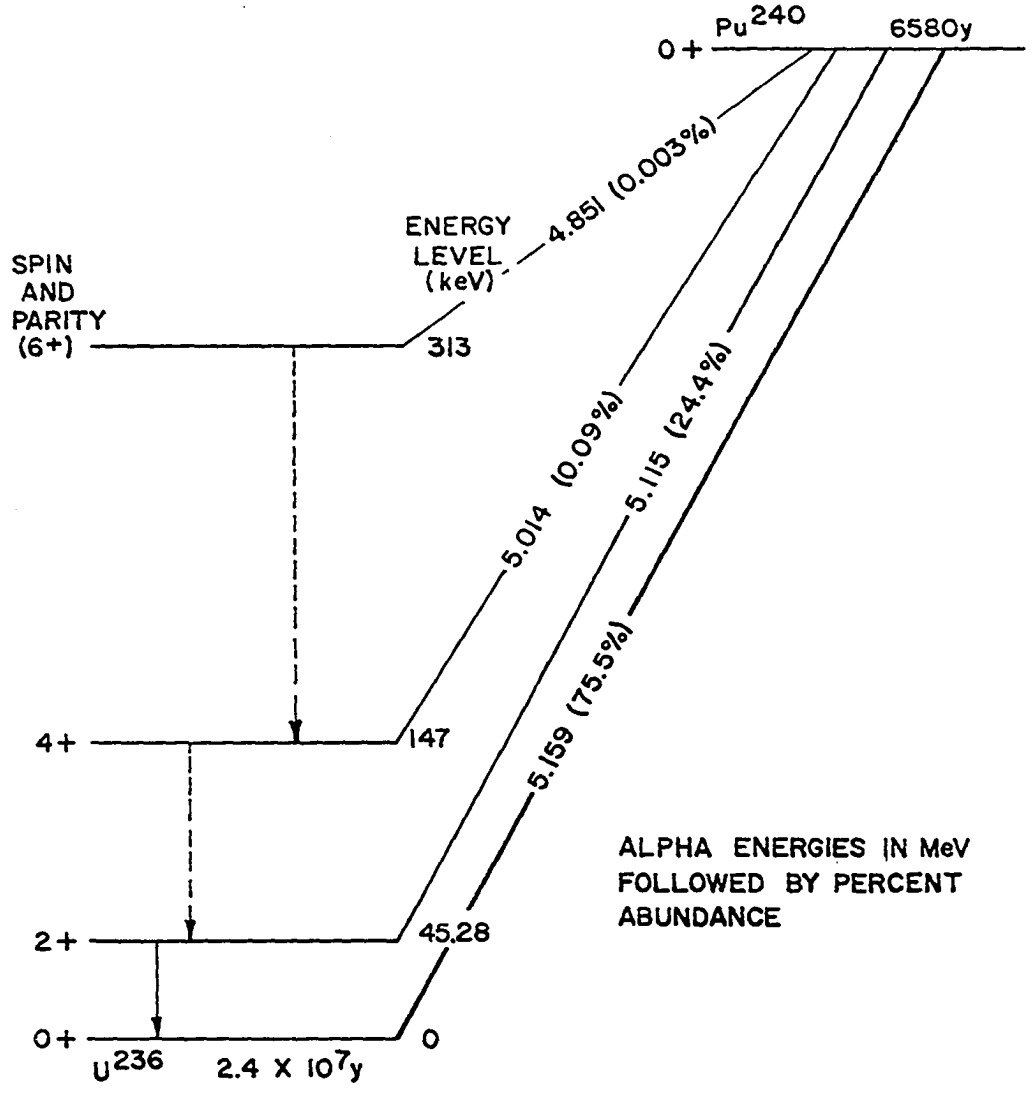

Fig. 1. Partial decay scheme of Pu-240

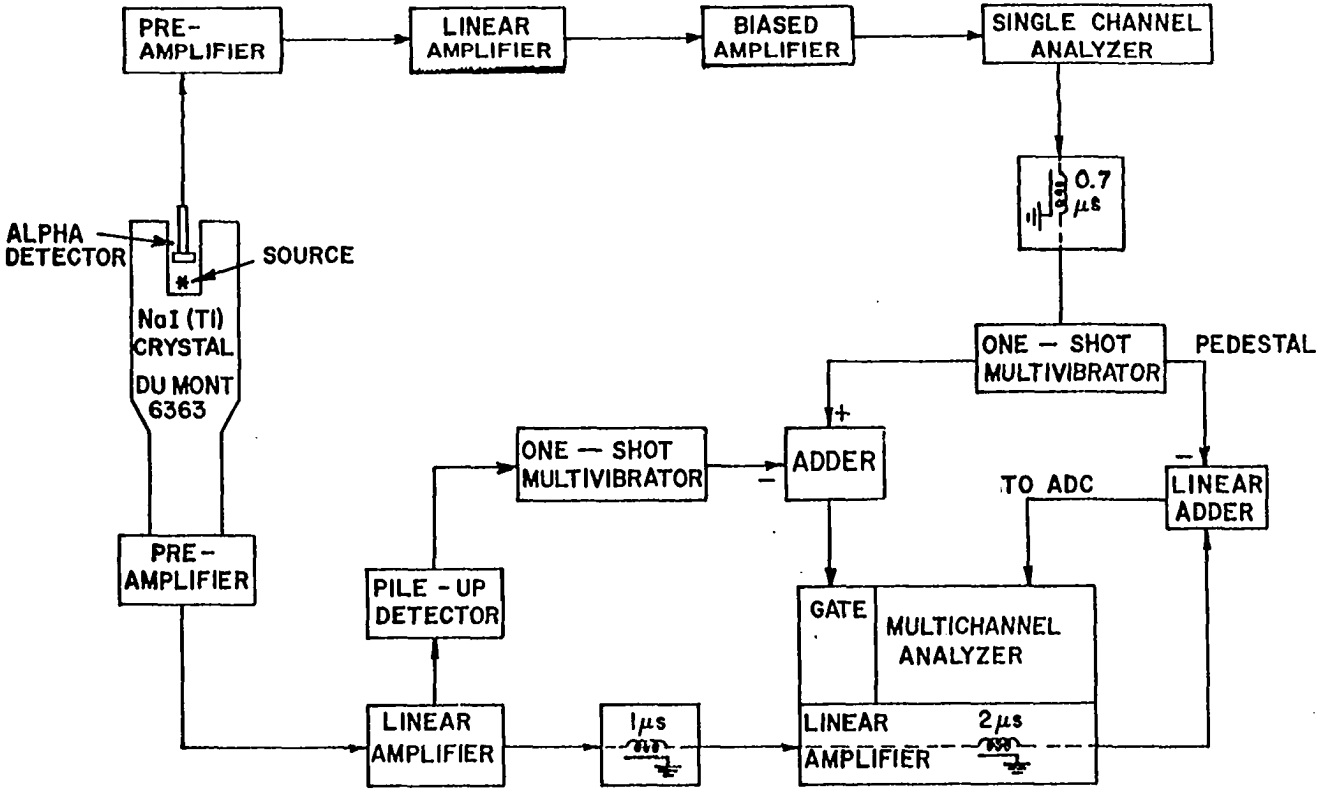

Fig. 2. Block diagram of equipment used for internal conversion coefficient measurement

shape and sent to the linear adder to be added to the pedestal pulse. The output of the linear adder was sent to the input to the ADC of the multichannel analyzer. The various delays shown in Fig. 2 were necessary to insure proper timing between pulses from the gating detector and pulses from the NaI(Tl) detector. The output from the double delay-line amplifier was also connected to a pile-up detector (see Appendix). Whenever any pulses distorted by pile-up were present, the pile-up detector triggered a one-shot multivibrator which generated a negative pulse of five microseconds duration. This negative pulse was summed with the smaller positive ADC gate pulse thus preventing the gate pulse from opening the ADC gate. The spectrum recorded by the multichannel analyzer was composed of a series of L X-ray peaks and a 45-keV gamma-ray peak (the transition energy of 45 keV was less than the threshold for internal conversion in the K-shell). However, before discussing this spectrum, some of the components of the above system and the performance of the gating detector will be discussed in more detail.

B. NaI(Tl) Detector and Source Assembly

The NaI(Tl) detector used for this experiment is a 2.75 in. x 3.00 in. crystal manufactured by Harshaw Chemical Company. The crystal has a 1.75 in. x 0.31 in. well which is lined with 0.015 in. of beryllium. The outside of this lining is covered with one micron of bright aluminum which serves to improve the light collection efficiency of the phototube. Since the efficiency of the crystal could be calculated accurately from a knowledge of the detector dimensions, it was important that all dimensions and tolerances of the crystal and its housing were known. These dimensions are shown in Fig. 3.

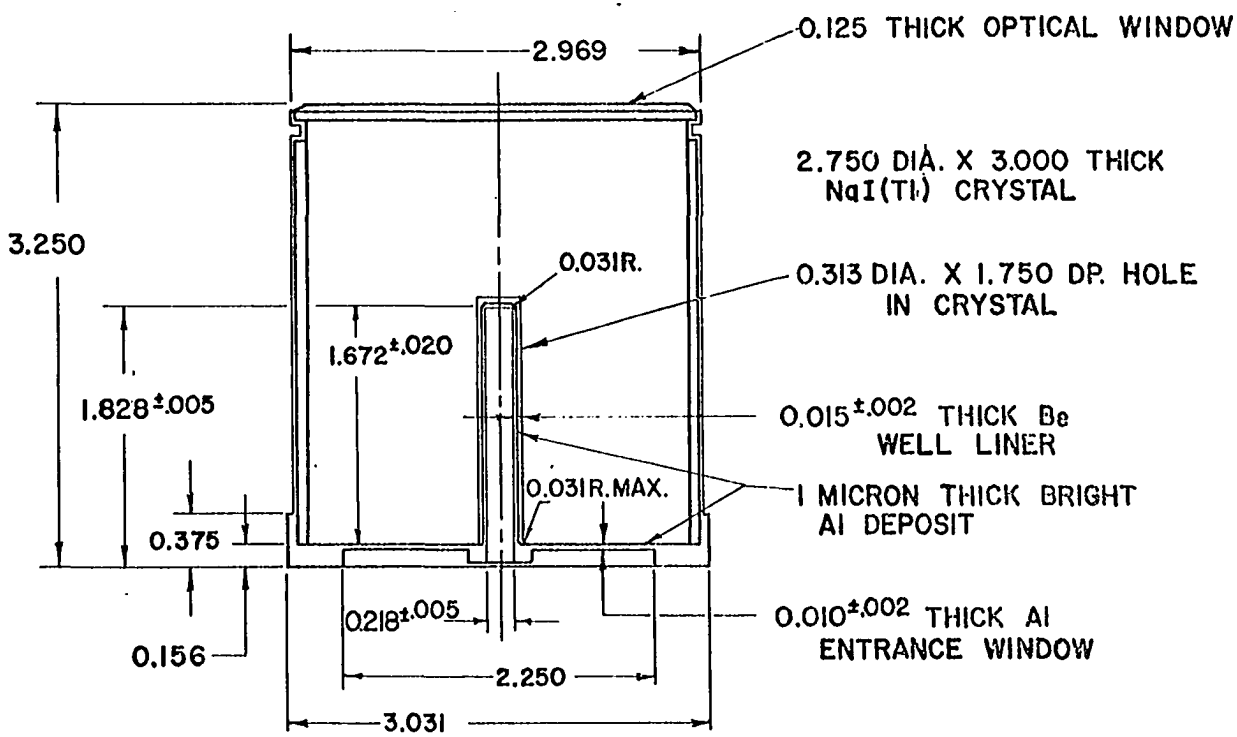

TOLERANCES: ±0.016 UNLESS OTHERWISE SPECIFIED
ALL DIMENSIONS IN INCHES

Fig. 3. Well-Type NaI(Tl) detector used in internal conversion coefficient measurement

The Pu-240 sources had a source strength of approximately 0.3 microcuries and were made on the Argonne National Laboratory Isotope Separator. The source backing was a thin disk of aluminized mylar, 0.200 in. (dia.) x 0.00025 in. (thick). The actual Pu-240 was deposited within a circle of radius 0.020 in. centered on the aluminum coated side of the mylar. Since a retarded beam was used on the isotope separator, these sources were quite thin, and very little degradation in alpha resolution due to source thickness was expected.

These sources could not be placed in the bare beryllium well because of the danger of contamination from the radioactive daughters of Pu-240 (these daughters are propelled out of the source backing due to the recoil from the alpha decay). Thus, an easily fabricated, removable liner was needed to contain the recoil nuclei. A simple solution to this problem was a closed-end cylinder made from 0.0005 in. mylar that would just fit inside the well. These mylar liners were made using a teflon rod as a support and Armstrong A4 epoxy to secure the mylar. The resulting liners were 0.205 in. (dia.) and could be made to any length desired. The source was placed in the bottom of the mylar cylinder. The alpha detector was positioned above the source by a teflon support at the open end of the liner, and the entire assembly was lowered into the well of the crystal. A diagram of this assembly before being placed in the NaI(Tl) detector is shown in Fig. 4. A major advantage of this type of construction was that the distance between the alpha detector and the source could be measured accurately.

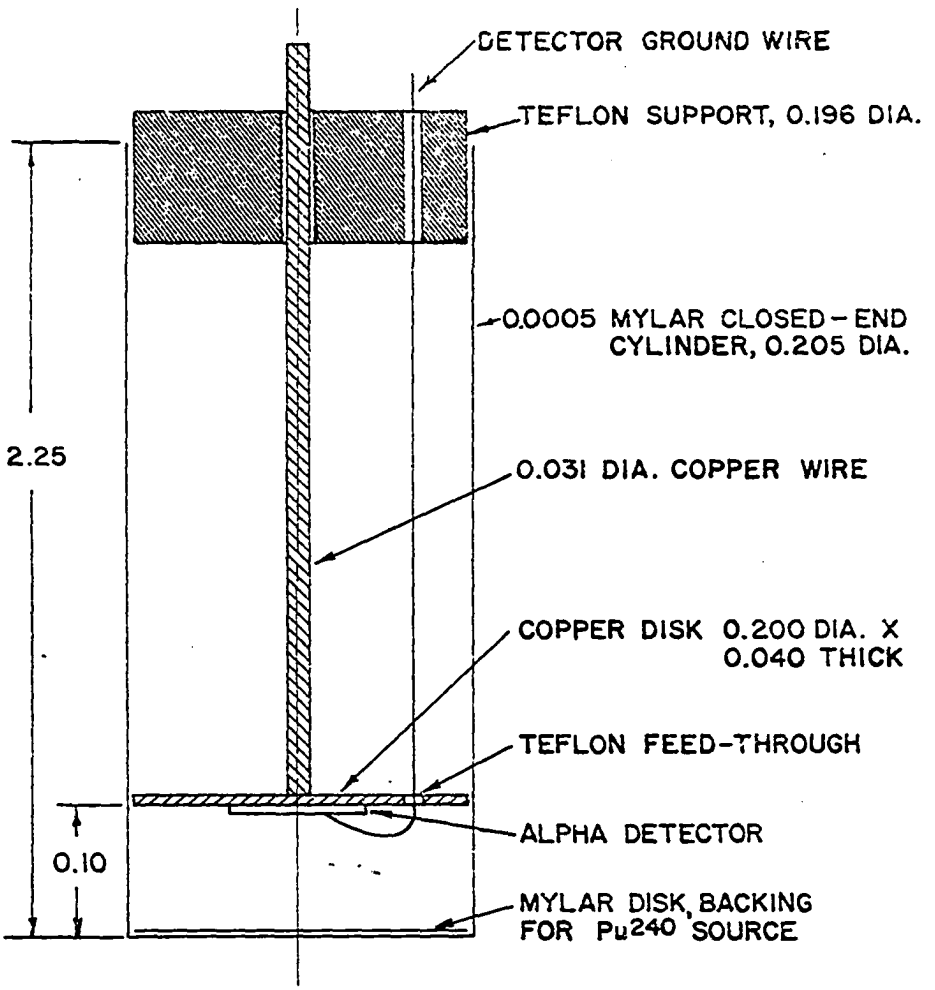

Fig. 4. Alpha detector and source assembly

C. Gating Detector

The silicon surface-barrier detectors used for gating purposes were manufactured by R.C.A., Ltd. of Montreal, Canada. Since the detector plus its mount must be small enough to be inserted into the mylar cylinder, no guard ring could be used. Thus the detector was mounted by R.C.A., Ltd. on a 0.200 in. (dia.) x 0.040 in. (thick) copper disk which was in turn attached to a 0.032 in. (dia.) copper wire. The copper wire served both as the signal lead for the detector and as a support for the copper disk. The copper disk also had a small teflon feed-through which supported the detector ground lead.

These small detectors worked surprisingly well. The best resolution (full width at half maximum) obtained was 17.5 keV with the source and detector in an evacuated chamber and using a preamplifier (Tennelec TC-130) having a field-effect transistor input stage. However, in this experiment the alpha detector could not be operated in a vacuum because the beryllium well lining would collapse. On the other hand, for an air atmosphere the resolution increased to 30 keV which was hardly suitable when the energy difference of the two alpha groups that must be resolved was 44 keV. Thus, a different atmosphere was necessary. Since alpha particles lose energy through ionization and excitation of the atoms in the absorber (42), a gas with a low electron density is desirable to avoid degradation of the alpha resolution. Helium gas represents the best practical environment. The resolution obtained in a helium atmosphere was 23 keV which was adequate to resolve the alpha groups.

To provide a suitable enclosure for the helium gas, a 2.0 in. (dia.) thin-walled aluminum cylinder was mounted on the NaI(Tl) detector. A

suitable feed-through for the alpha-detector signal lead and an entrance port for the helium gas were provided through the cylinder walls. The end of the cylinder could be capped to prevent escape of any helium gas. Since some helium leaks were present in this system, a helium gauge pressure of one to two inches of water was continually maintained; a resolution of about 23 keV was obtained for time periods up to 14 days.

D. Alpha Spectrum Analysis

One of the assumptions made in the development of the coincidence method was that the gating detector must provide a unique gate for the transition of interest. In the decay of Pu-240, there is an intense ground-state alpha group at 5.159 MeV, only 44 keV above the 5.115-MeV alpha group (these alpha groups will be subsequently referred to as the α_o group and the α_1 group, respectively). Thus, because the alpha detector resolution was 23 keV, a correction was made for any pulses due to α_o-group particles detected within the window set by the single channel analyzer. Actually, this correction was much larger than expected. The pulse height spectrum from the detection of monoenergetic alpha particles by this type of surface-barrier detector was an asymmetrical peak with a low-energy tail extending about 100 keV below the center of the peak. The presence of this low-energy tail resulted in significant detection of α_o-group particles in the single channel analyzer window. Fortunately, no transitions were in coincidence with the α_o group so that unwanted gamma rays or X-rays were not gated into the photon spectrum, and the only necessary correction to the photon spectrum was for the pedestal peak (a count was registered in the pedestal peak every time the gate to the ADC was opened with no pulse from the NaI(Tl) detector present). In order to perform this correction, a detailed analysis of the

alpha pulse height spectrum was necessary.

Normally, in unfolding pulse height spectra, a least squares computer analysis is made in which a given function (response function) describes each peak in the spectrum. This response function may be the same for all the peaks, or it may be a function of the peak location in the pulse height distribution. In the present investigation, a Fortran computer program written by R. S. Dingus was used in which the response function was the sum of a Gaussian peak and three non-Gaussian peaks. Each non-Gaussian peak, described by nine parameters, was a very general function that could assume many different shapes with the proper choice of parameters. No attempt will be made to describe this program as it has been adequately described elsewhere (40). The method used to unfold the alpha spectrum required that the shape of the α_1 group be determined as described in the next paragraph.

Because of the simplicity of the Pu-240 decay scheme, an experimental pulse height spectrum of the α_1 group could be obtained. Since all but a negligible fraction of the X-rays and gamma rays for this source occur as the 45-keV level is de-excited and since the lifetime of the 45-keV level is 2.32×10^{-10} sec. (24), the detection of an X-ray or gamma ray implies that an α_1-group particle has just been emitted. Thus, to produce the α_1-group spectrum, the roles of the NaI(Tl) detector and the alpha detector were reversed. Pulses from the well crystal were used to open the ADC gate whenever X-rays or gamma rays were detected, and the alpha spectrum was recorded by the multichannel analyzer. Therefore, a gated alpha spectrum was produced which contained only the α_1 group (this spectrum will subsequently be referred to as the gated alpha spectrum). At the beginning of each

data run, a gated alpha spectrum using this method was obtained, and a least squares computer analysis was performed. The appearance and the resulting computer fit for a typical gated alpha spectrum is shown in Fig. 5.

As can be seen, the computer fit was quite good with the variance of the fit equal to 1.19 (chi-square over degrees of freedom; for an ideal fit the variance of the fit is 1.00). Four peaks are seen in the spectrum. The largest is a pure Gaussian and represents the full-energy peak. The low-energy tail occurs to the left of the Gaussian. The non-Gaussian peak under the low-energy tail shows that that the function being used to fit the low-energy tail does not have quite enough structure to provide a good fit over this region of the spectrum. In fact, the amplitude of this peak is a function of the number of channels that are included in the low-energy tail. It was impossible to achieve a good fit with only two non-Gaussian peaks below the full-energy peak when more than 60 channels were included in the tail (at the same gain settings used for the spectrum in Fig. 5). The non-Gaussian peak above the full-energy peak might possibly be attributed to the summing of alpha particles with conversion electrons; however, as will be discussed later, this peak was also present for alpha groups in which no coincident conversion electrons were present, e.g. the α_o group.

To complete the alpha spectrum analysis, a series of singles alpha spectra (obtained without gating)were taken at various times during each data accumulation period. By knowing the shape of the α_1 peak from the gated spectrum analysis, an accurate computer analysis for the singles spectra was possible. A typical singles alpha spectrum is shown in Fig. 6.

For this case a reasonable computer fit was more difficult to obtain since the set of parameters that produced a good fit was not unique. For

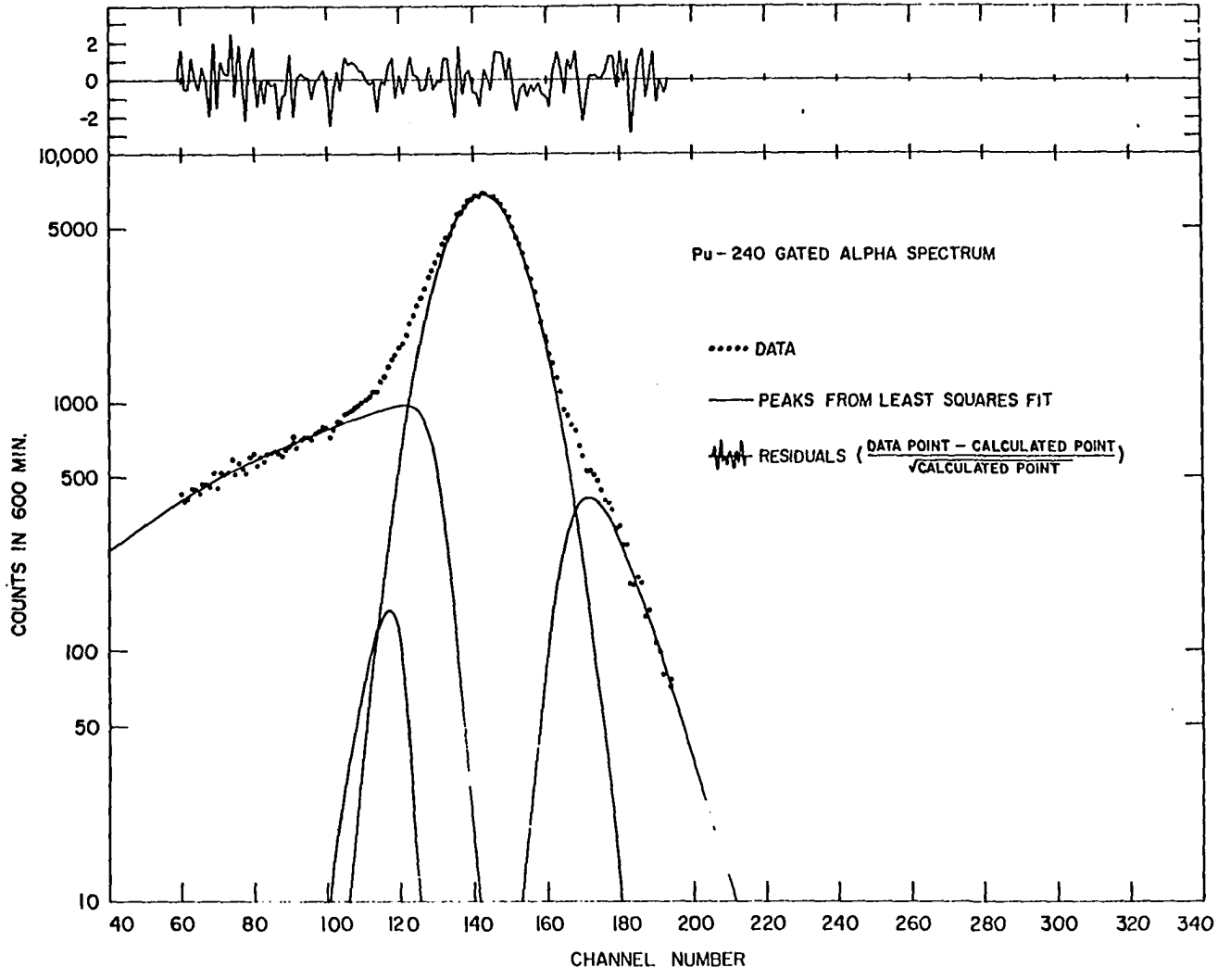

Fig. 5. Gated alpha spectrum of Pu-240

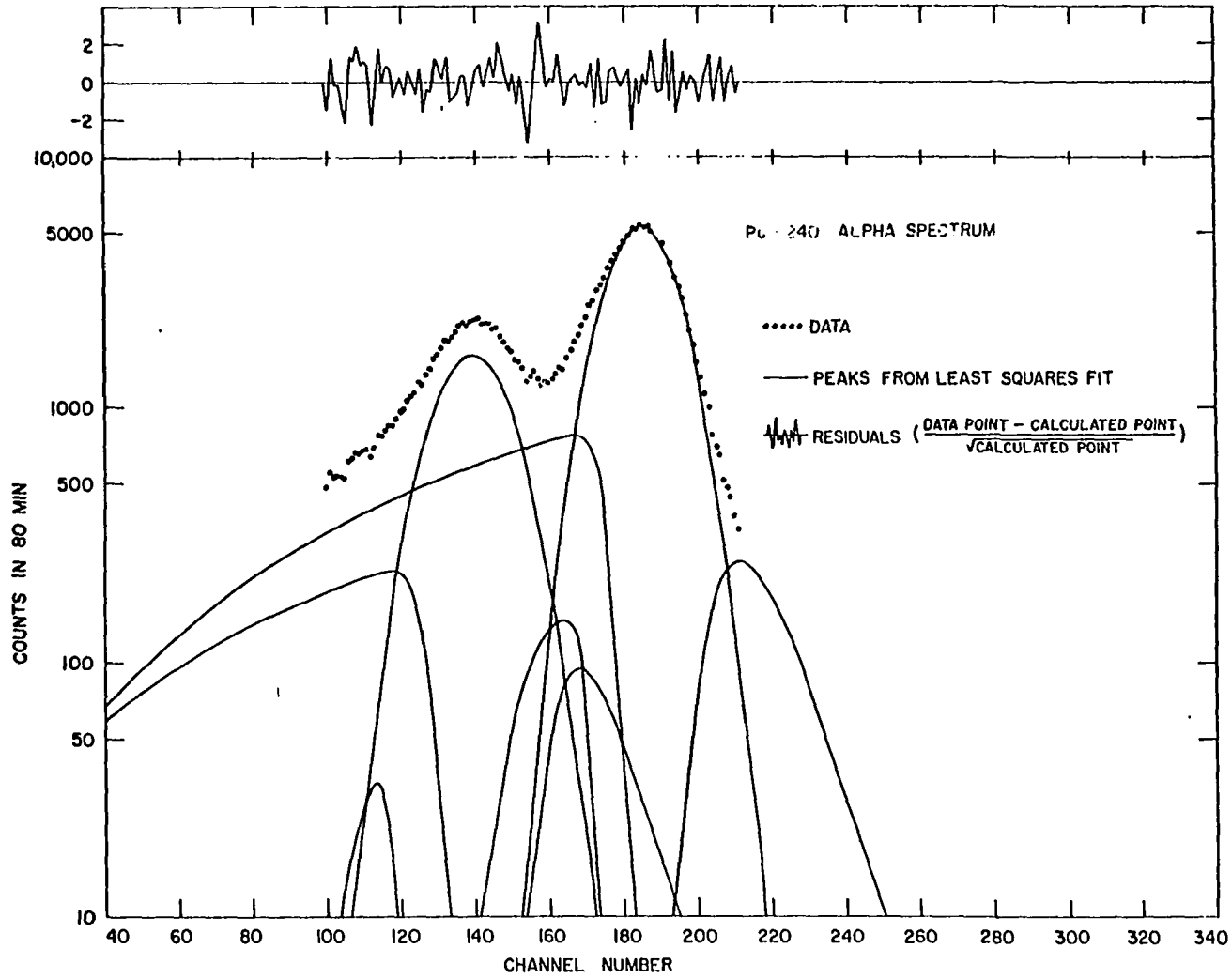

Fig. 6. Singles alpha spectrum of Pu-240

this reason, various constraints were added to the program. The amplitudes of the non-Gaussian sections of the α_1 peak were fixed relative to the α_1 Gaussian amplitude which was the only parameter of the α_1 peak allowed to vary in the least squares analysis. Thus, the shape of the α_1 peak was held constant while its amplitude could vary. By allowing various parameters of the α_o peak to vary also, a fit was obtained which yielded the experimentally measured absolute intensity of the α_1 group, 24.4 percent (41). In general, a good fit could be obtained for α_1 intensities from 22 percent to 26 percent. Since the position of the single channel analyzer window across the α_1 peak was known, the relative contribution of the α_o low-energy tail to the gating could be determined accurately. For the spectrum in Fig. 6, the α_1-to-total ratio for the gating channels, 60 through 160, was 55.4 percent.

As can be seen in Fig. 6, the complete alpha spectrum was not used in the computer analysis. Only 60 channels were included in the α_o low-energy tail. The calculated curves shown below channel 100 were an extrapolation of the computer fit. The extrapolation was fairly accurate; however, the sum of the extrapolated values for each channel was about two percent less than the experimental values (the data points for this region are not shown in Fig. 6 since they were not used in the computer fit). In order to obtain an accurate fit for this region, the extrapolated portion of the α_1 low-energy tail was assumed to be correct since its shape was obtained by an analysis of the gated alpha spectrum. The contribution from the α_o tail below channel 100 was obtained by subtracting the α_1 tail from the experimental value for each channel in this region.

The effect of summing between the conversion electrons and the α_1-

group particles can be described from the analysis of the alpha spectra. The height of the non-Gaussian peak above the full-energy (Gaussian) peak relative to the Gaussian amplitude was approximately the same for both alpha peaks, and the width of the α_1 full-energy peak was always 0.75 to 1.50 keV greater than the width of the α_0 full-energy peak.

The assumption that conversion electrons were responsible for this increase in width is reasonable because the pulses produced by the detection of the conversion electrons were about a factor of 50 smaller than the pulses produced by the detection of the alpha particles. The main effect of the summing even for a transition with a large internal conversion coefficient should be to broaden the peak slightly, as observed.

From a series of these least squares fits, several statements can be made about the performance of the alpha detector. The low-energy tail-to-total ratio for a single alpha peak was 15 percent when the source and detector were in an evacuated chamber. This ratio increased to 22 percent in a helium atmosphere. Thus, energy losses by the alpha particle in the helium gas and possible scattering from the walls of the mylar liner caused the tailing to increase by seven percent (other less important contributions to the low-energy tail are given in Reference 43). Finally, after 10^9 - 10^{10} alpha particles had been detected, the resolution of the alpha detector began to deteriorate. This deterioration could be retarded by increasing the bias voltage, but in general no more extended data runs could be made.

E. Efficiency of the NaI(Tl) Detector

The efficiency, $\epsilon(E)$, of the NaI(Tl) detector is defined as the probability that a gamma ray of energy E, emitted from a point source

positioned along the axis of a cylindrical well-type NaI(Tl) detector, will lose some energy in the crystal. The integral expression for $\epsilon(E)$ is

$$\epsilon(E)=\frac{1}{2}\int_0^{\theta_0} \exp\{-\alpha_2(E)D_2(\theta)-\alpha_3(E)D_3(\theta)\}[1-\exp\{-\alpha_1(E)D_1(\theta)\}]W(\pi-\theta)\sin\theta d\theta \qquad (12)$$

where $\alpha_1(E)$ is the total (minus coherent) attenuation coefficient of the crystal, $\alpha_2(E)$ and $\alpha_3(E)$ are the photoelectric absorption coefficients for the beryllium well lining and copper disk, respectively, measured in the direction of zenith angle θ as shown in Fig. 7[1].

The first factor in the integral represents the probability that a photon will penetrate the copper disk and well lining (of course θ will have values such that the photon is not incident on the copper disk). The second factor is the probability that the photon will deposit some energy in the crystal, and the third factor, $W(\pi-\theta)$, is the probability that a gamma ray will be emitted into solid angle $d\Omega$ at polar angle $\pi-\theta$ following alpha decay along the direction $\theta=\pi$[2]. To perform the integration, a Fortran computer program (40) was used after modification to include $W(\theta)$. The original program has been verified to be accurate to 0.1 percent for low-energy photons.

For an alpha-gamma cascade such as the $0^+ \xrightarrow{\alpha} 2^+ \xrightarrow{\gamma} 0^+$ cascade in the decay of Pu-240, $W(\theta)$ assumes the simple form

$$W(\theta) = 1 + A_2P_2(\cos\theta) + A_4P_4(\cos\theta). \qquad (13)$$

If no correlation perturbations are present, the coefficients A_2 and A_4 can be calculated in a straightforward manner to be 0.714 and -1.714 res-

---

[1]The absorption of photons in the mylar liner and alpha detector is ignored.

[2]From parity considerations $W(\pi-\theta)$ is equal to $W(\theta)$, and $W(\pi-\theta)$ will subsequently be referred to as $W(\theta)$.

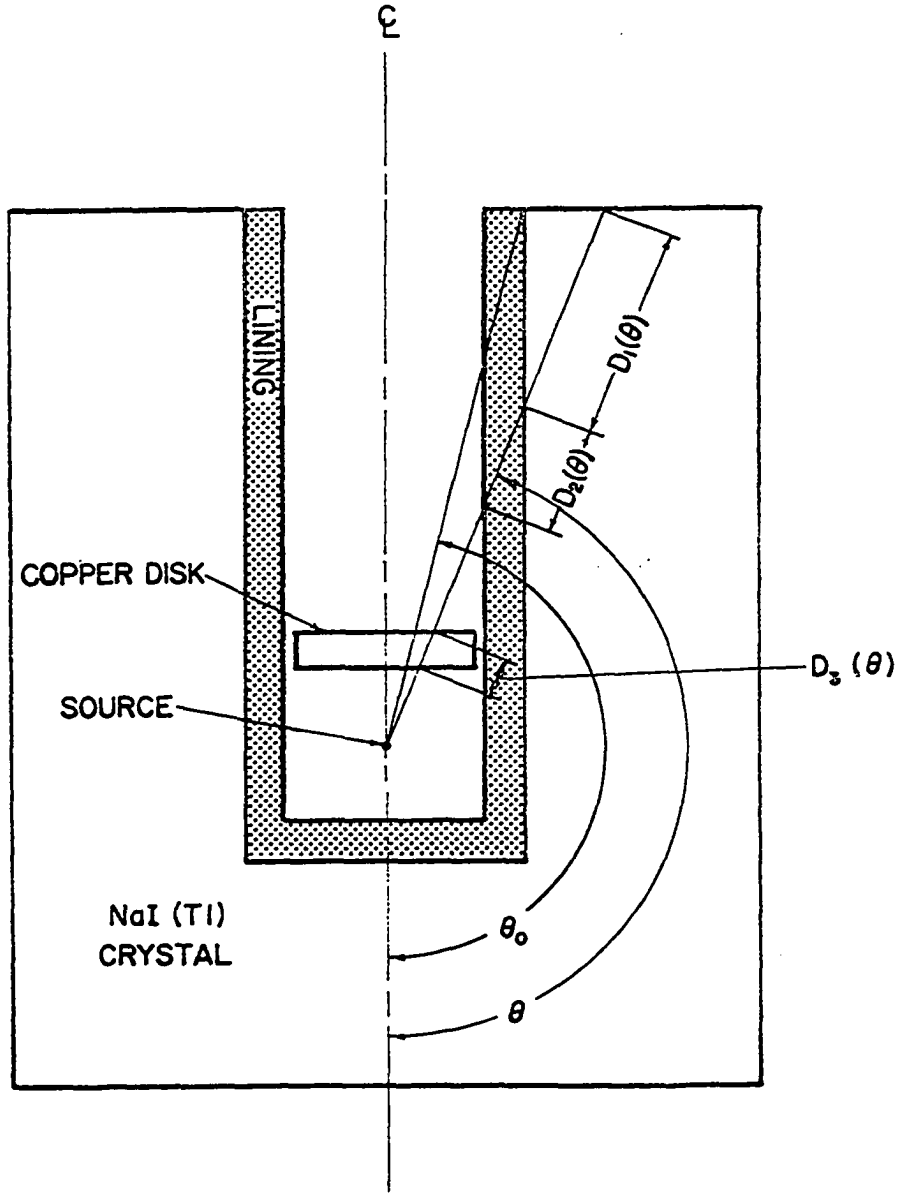

Fig. 7. Detector configuration used for efficiency calculation

pectively (44)[1]. Several measurements have been made for cascades of this type in the very heavy elements (45), and in all cases A_2 and A_4 were found to be less than the theoretical values indicating that the correlation is perturbed. Unfortunately, the coefficients for the Pu-240 cascade have not been measured. Thus, the experimental values (46) of A_2 and A_4 for the $0^+ \xrightarrow[\alpha]{} 2^+ \xrightarrow[\gamma]{} 0^+$ cascade in the decay of Pu-238 were used in the efficiency calculations. The assumption that these coefficients are the same as the coefficients in the Pu-240 cascade does not introduce a large error into the efficiency calculation for the following reasons. First, the efficiency is a slowly-varying function with respect to changes in A_2 and A_4 so that a large uncertainty in the coefficients does not introduce a large uncertainty in the efficiency. Second, a series of efficiency calculations were made using the values of A_2 and A_4 from all reported angular correlation measurements of $0^+ \xrightarrow[\alpha]{} 2^+ \xrightarrow[\gamma]{} 0^+$ cascades in even-even nuclei with $A > 224$ (45), and the calculated efficiencies agreed to within one percent. Thus, a one percent uncertainty due to possible errors in the values for A_2 and A_4 was assigned to the efficiency.

Before the efficiency calculation can be completed, the values for A_2 and A_4 must be corrected for the finite size of both the alpha detector and the Pu-240 source. The correlation function, $W(\theta)$, must be averaged over both the solid angle subtended by the alpha detector and the area of the source to obtain an average correlation function, $\overline{W}(\theta)$, to be used in the efficiency calculation. Thus, for cylindrical symmetry,

---

[1]The parameters A_2 and A_4 are functions of the angular momenta and parity of the three levels and, hence, do not depend on the energy difference between the levels. Thus, A_2 and A_4 are theoretically the same for all cascades of this type.

$$\bar{W}(\theta) = \frac{\int_o^r \rho d\rho \int_{\Omega(\rho)} W(\beta)\, d\Omega}{\int_o^r \rho d\rho \int_{\Omega(\rho)} d\Omega} \qquad (14)$$

where r is the radius of the source, $\Omega(\rho)$ is the solid angle subtended by the alpha detector from a point on the source a distance ρ from the center, and β is the angle between the direction of emission of the photon and the direction of the alpha particle which is ejected into $d\Omega$. Fortunately, for cascades of this type, the form of the correlation is unchanged in the averaging process, and Valladas et al. (47) have performed this integration for the case of a cylindrically symmetric alpha detector and source having a common axis of symmetry. Their calculations show that with an alpha detector radius of 0.032 in., a source diameter of 0.020 in., and a source-to-detector distance of 0.10 in., A_2 and A_4 are attenuated by factors of 0.918 and 0.763, respectively. The shape of the correlation function is shown in Fig. 8. The line $W(\theta) = 1$ corresponds to an isotropic photon distribution.

A final correction to the efficiency results from the finite size of the source. If a photon is emitted from the source at a point not on the crystal symmetry axis, the solid angle subtended by the copper disk is slightly smaller than that subtended by a source point on the symmetry axis. This effect is not calculated easily since the efficiency integral would have to be changed to an off-axis double integration. However, with a source size of 0.04 in. (dia.), a source-to-detector distance of 0.10 in., and the assumption of no further effects from angular correlation, an upper limit of one percent can be placed on the effect of the correction on the efficiency. For this reason, the calculated efficiency was increased one

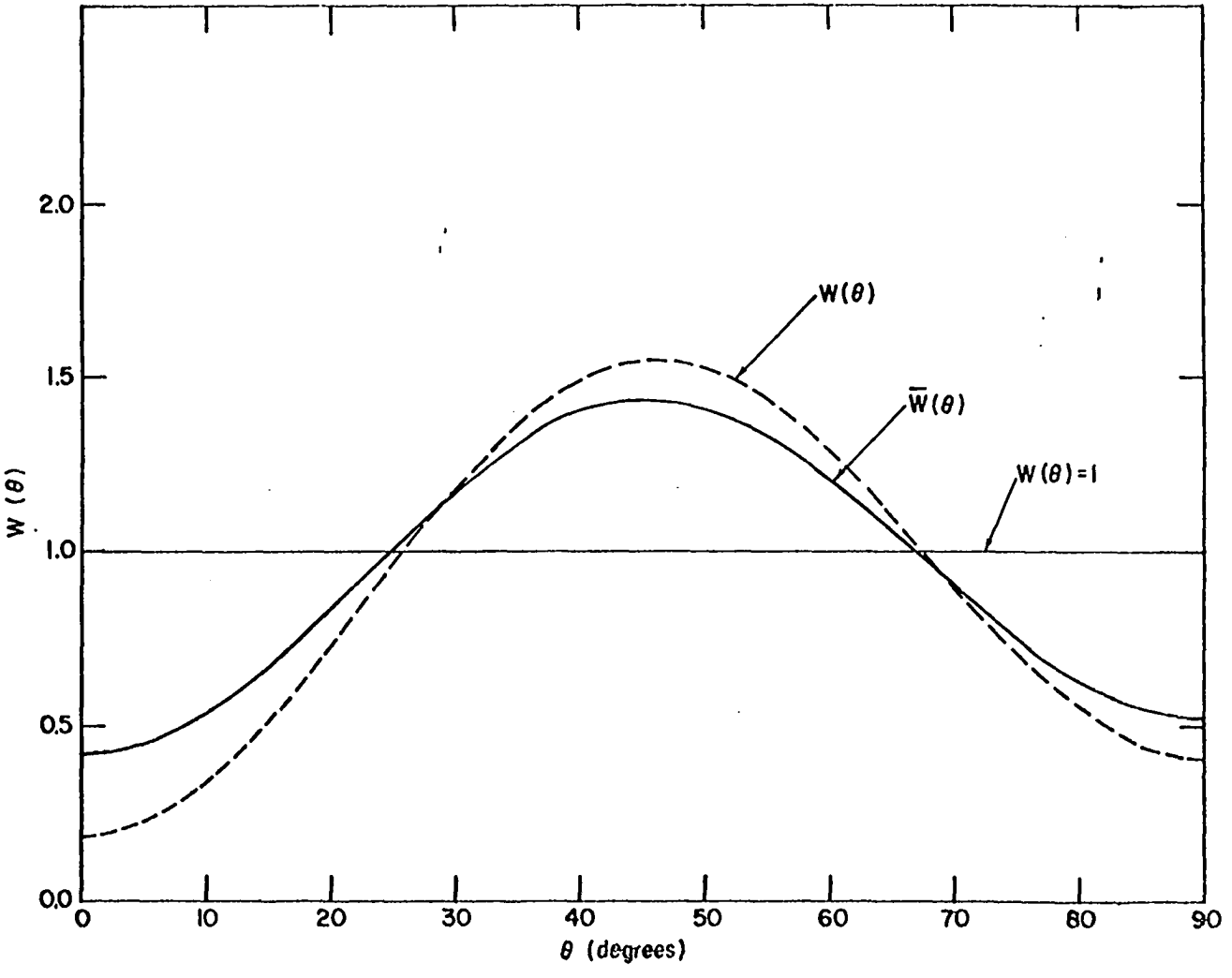

Fig. 8. Pu-238 angular correlation functions compared with W(θ) = 1

percent and assigned an uncertainty of one percent.

The results of the efficiency calculations for a photon energy of 45 keV are given in Table 1. Q_2 and Q_4 are the attenuation coefficients for A_2 and A_4, respectively, from the finite size corrections. $\epsilon(45)$ is the efficiency calculated for a photon energy of 45 keV according to the correlation function used in the efficiency integral. The absorption coefficients were taken from the report of G.W. Grodstein (48). As can be seen the efficiency is a slowly-varying function of A_2 and A_4. The uncertainty listed with each efficiency is a statistical combination of the two uncertainties discussed earlier along with a one percent uncertainty resulting from the measurement of the position of the alpha detector relative to the source.

Table 1. Gamma-ray efficiencies for various values of A_2 and A_4

Correlation Function	A_2	A_4	Q_2	Q_4	$\epsilon(45)$
$\bar{W}(\theta)_{theor.}$	0.714	-1.714	0.918	0.763	0.839 ± 0.017
$\bar{W}(\theta)_{Pu\text{-}238}$	0.330	-1.145	0.918	0.763	0.861 ± 0.017
$W(\theta) = 1$	0.0	0.0	-	-	0.872 ± 0.017

F. Response of the NaI(Tl) Detector to Low-Energy Photons

As discussed in Chapter IV, a knowledge of the photon response of the NaI(Tl) detector is necessary to determine the photon intensities. In this section the response for low-energy photons will be discussed in detail and a measurement of the photopeak-to-total ratio at two photon energies will be reported.

The escape of iodine K X-rays from the NaI(Tl) crystal following the photoelectric absorption of low-energy photons creates a prominent Gaussian peak (escape peak) 29.2 keV below the photopeak (the average K X-ray energy for iodine is 29.2 keV). For a source outside of the well of the NaI(Tl) crystal, the ratio of the escape-peak intensity to that of the photopeak is 17 percent for 45-keV photons (49). By placing the source in the well, this ratio decreases to four percent since many of the K X-rays that escape from the crystal surface are reabsorbed by the crystal.

Similarily, a significant fraction of the low-energy photons are photoelectrically absorbed in the configuration placed in the detector well. Thus, K X-rays characteristic of such absorption are created and may interfere with the analysis. , experiment the highest-energy X-rays that could be created in this manner were 8.0 keV from photoelectric absorption in the copper disk supporting the alpha detector. These 8.0-keV X-rays did not interfere with the analysis because their sole effect was to broaden the pedestal peak.

The low-energy photons are also Compton scattered in the NaI(Tl) crystal, and the resulting secondary photons can escape, with a net deposition in the NaI(Tl) crystal of 0 keV (scattered through 0 degrees) to 6.8 keV (scattered through 180 degrees) for an incident photon energy of 45 keV. At this photon energy the probability for Compton scattering in NaI is about a factor 100 less than the probability for photoelectric absorption in NaI (48). In addition, with the use of a well-type crystal there is a very high probability that any Compton scattered photons will be absorbed in the crystal.

Likewise, the photons are Compton scattered in the configuration placed

in the detector well, and the secondary photons may be detected by the NaI(Tl) detector. For 45-keV photons the secondary photon energies range from 38.2 keV (for scattering through 180 degrees) to 45 keV (for scattering through 0 degrees). Again the principal source of this scattering is the copper disk. Although for a photon energy of 45 keV the probability for Compton scattering in copper is about a factor of 50 less than the probability for photoelectric absorption, this effect can contribute to the events below the photopeak.

Since most low-energy interactions occur near the surface of the NaI(Tl) crystal, some of the light pulses produced are attenuated upon scattering at the surface of the crystal (the half-thickness for a 45-keV photon in NaI is 0.004 in.). This effect, resulting in a low-energy tail to the photopeak, was studied by Eldridge and Crowther (50) as a function of the surface treatment of the NaI(Tl) crystal. They observed that the smallest effect occurred for a polished crystal surface (surface scratches are normally added to improve the high-energy resolution). Thus, to minimize this cause of distortion of the photopeak, the crystal used in this experiment had a highly-polished well surface.

Since all of the above effects result in events below the photopeak, the photopeak-to-total ratio was determined for photon energies of 58 and 45 keV. The spectra used to determine these ratios will now be discussed. The K X-ray spectrum from electron capture in W-181 is shown in Fig. 9a. The K_α(57.5 keV) and K_β(65.2 keV) peaks are unresolved, the prominent peak being that of the K_α X-ray (the K_β X-ray intensity is 0.330 times the K_α intensity). The low-energy tail is clearly visible on the left-hand side of the K_α peak when the data points are compared to the Gaussian curve

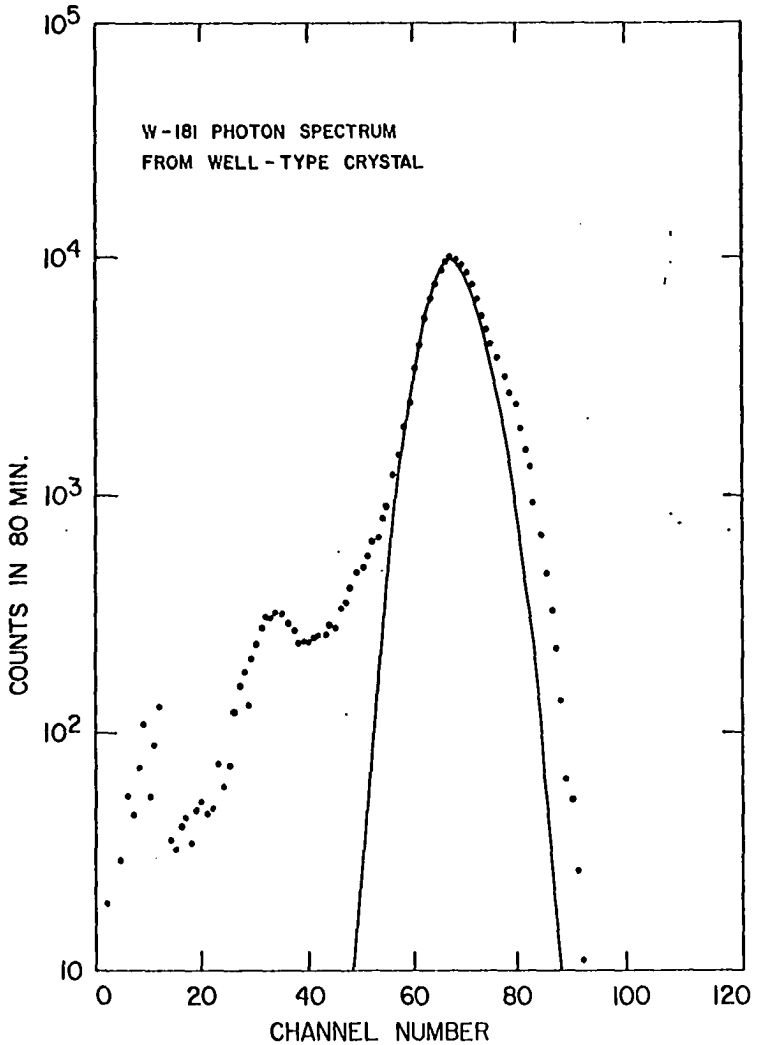

(a) W-181 K X-ray spectrum

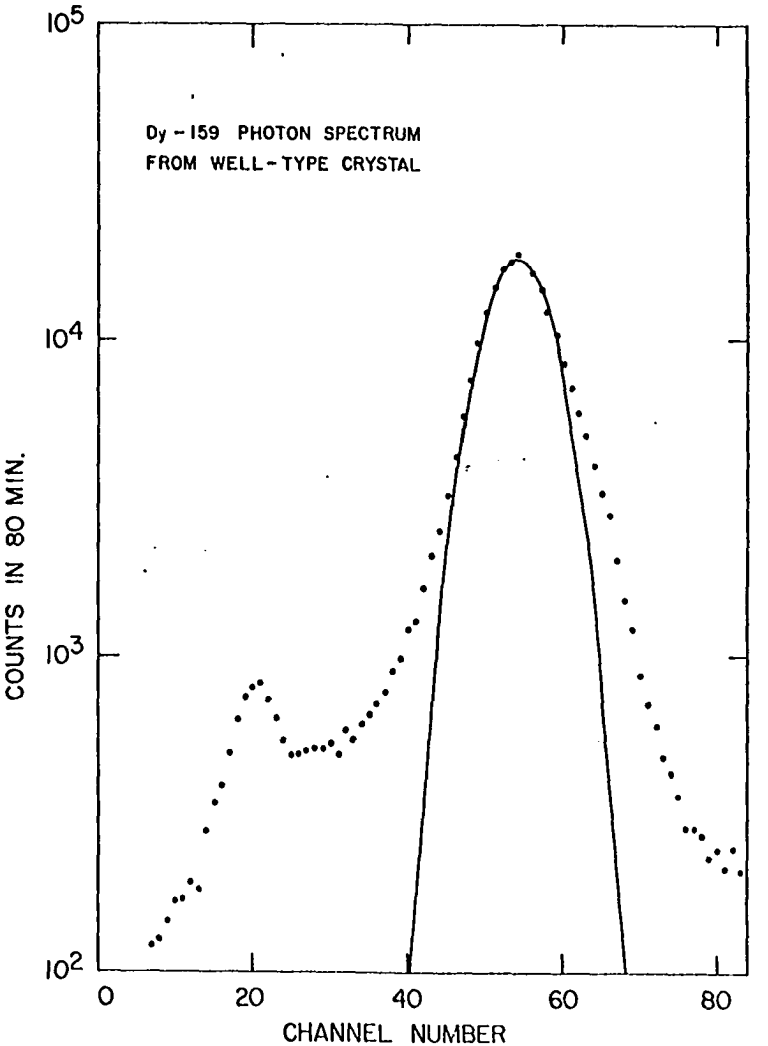

(b) Dy-159 K X-ray spectrum

Fig. 9. Photon spectra used to determine the photopeak-to-total ratio at 45 keV

representing the K_α photopeak. The K_α escape peak at 28.3 keV is seen in channel 34. After a small correction was made for the K_β low-energy tail, the photopeak-to-total ratio was found to be 0.927 $\pm$ 0.016.

The photon spectrum from electron capture in Dy-159 is shown in Fig. 9b. In addition to the K_α(44.5 keV) and K_β(50.4 keV) peaks, there is indication of the low-intensity 58-keV gamma rays from Tb-159 in channel 68. Since the W-181 spectrum yielded a photopeak-to-total ratio applicable to this 58-keV gamma ray, an analysis of the photon spectrum from the decay of Dy-159 gives a photopeak-to-total ratio at 45 keV of 0.901$\pm$0.016. The ratios at 45 and 58 keV are approximately equal and may be compared to the results of a more extensive sutdy at higher energies by Dingus *et al.* who showed that the ratio for a similar well-type crystal was independent of energy from 58 keV to 145 keV (40).

G. Gated Photon Spectrum Analysis

The analysis of the Pu-240 gamma-ray spectra in coincidence with the α_1 group was much simpler than the alpha spectrum analysis discussed earlier. Only one gamma ray, well separated from the L X-ray peak in the pulse height distribution, was gated into the spectrum. Although the photon spectrum was not complicated, several problems, normally unimportant, became critical in this experiment.

Since the L-shell internal conversion coefficient for this transition was approximately 400, the intensity of the 45-keV gamma rays was much less than that of the L X-rays. Thus, pile-up from the L X-rays could severely distort the 45-keV photopeak. As discussed in the Appendix, a large fraction of the piled-up pulses was eliminated by the use of a pile-up detector.

Because of the low counting rate, the accumulation period of data

was as long as 10 to 12 days in order to obtain a statistically meaningful number of gamma-ray events. Thus, any small drifts in the electronics could become important sources of distortion of the 45-keV photopeak. To minimize drifts precision resistors were used in the voltage divider for the photo-tube, and the room temperature was carefully regulated. Also, at least once every eight hours, an Am-241 gamma-ray spectrum was recorded (Am-241 has a high-intensity 60-keV gamma ray). By observing the change in the location of the 60-keV photopeak, the amount of drift could be determined. Normally, the change in the 60-keV peak location was less than three channels over a 14-day period, and under favorable conditions the change was less than one channel. Fortunately, this drift occurred gradually and never in an oscillatory manner so that the 45-keV gamma peak was only broadened slightly.

A typical Pu-240 gated spectrum is shown in Fig. 10. The three main peaks are the pedestal peak, L X-ray peak, and the 45-keV gamma-ray peak. As can be seen, the intensity of the gamma ray is much less than the X-ray intensity. The shape of the gamma-ray peak is distinctly non-Gaussian because the high-energy tail of the X-ray peak extends under the low-energy side of the 45-keV photopeak. Thus, before the area of the photopeak can be determined, the X-ray tail has to be separated from the gamma-ray peak.

The simplest method to determine the area of the 45-keV photopeak is to fit a Gaussian curve to the right-hand side of the peak and then extrapolate it to the left-hand side. The Gaussian peak shown superimposed on the gamma-ray peak was obtained in this manner. This method should be very accurate because no events from the summing of two L X-rays can occur above 42-keV (all of L X-ray groups have energies less than 21 keV, and higher-order

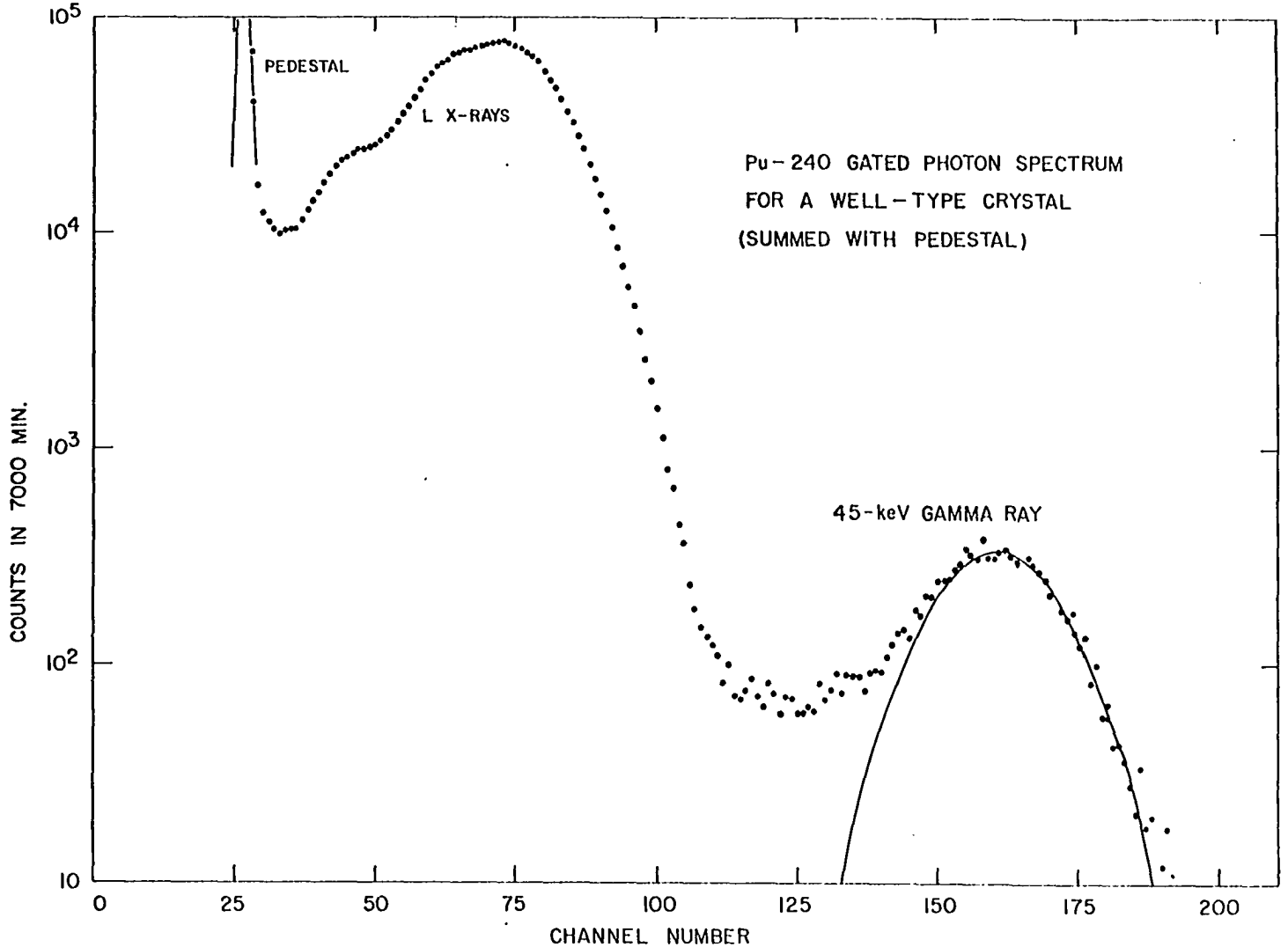

Fig. 10. Gated photon spectrum of PU-240

summing can be ignored).

The area of the photopeak can also be obtained by subtracting the X-ray tail from the gamma-ray peak. The assumed shape of the X-ray tail is not extremely important since a 20 percent error in the area of the tail under the gamma-ray peak results in only a three percent error in the photopeak area. The photopeak area obtained in this manner agreed to within two percent of that obtained by fitting a Gaussian curve to the right-hand side of the peak.

After determining the photopeak area, the total number of gamma-ray events can be found since the photopeak-to-total ratio at 45 keV is known. Also, as explained in Chapter IV, N_o is the total area of the photon spectrum plus pedestal peak. For the spectrum shown in Fig. 10, N_o/N_γ is 1686 ± 129.

H. Final Results

Three sets of gated Pu-240 spectra were taken and analyzed as discussed in the previous section. Two sets of data were accumulated for 12 days and a third for five days. The same geometry was used with all sets with the exception that the distance from the Pu-240 source to the alpha detector was decreased for each subsequent data accumulation period. Thus, the major difference in these three spectra was the gating count rate; the rate of the third set was approximately four times that for the first set. However, the advantages gained by a higher counting rate were somewhat offset by an increase in the alpha-peak width as the source-to-detector distance was decreased.

The quantities used to determine the total internal conversion coefficient for each data set are given in Table 2. All of the entries have been discussed previously with the exception of $\overline{\alpha_1/(\alpha_1 + \alpha_o)}$ which is an

average of the various α_1-to-total ratios obtained from the analyses of the alpha spectra for each data accumulation period. As can be seen, the largest uncertainty is for N_o/N_γ and is a direct result of the low intensity of the 45-keV gamma rays. The total internal conversion coefficient for each data set was obtained from equation 6.

Table 2. Total Internal Conversion Coefficient from each Data Period

Data Period	N_o/N_γ	$\overline{\alpha_1/(\alpha_1+\alpha_o)}$	$\epsilon(45)$	α
1	1289 ±100	0.549 ±0.010	0.871 ±0.015	615 ±49
2	1360 ±93	0.537 ±0.020	0.832 ±0.014	606 ±48
3	1686 ±129	0.476 ±0.020	0.750 ±0.013	601 ±54

The final internal conversion coefficient was taken to be the average of the three internal conversion coefficients from the three data sets. The resulting total internal conversion coefficient for the 45-keV E2 transition in U-236 is

$$\alpha = 607 \pm 29. \qquad (15)$$

The error assignment is to be interpreted as a standard deviation and was obtained by standard statistical methods from individual uncertainties.

VI. COMPARISON WITH THEORY

In order to obtain useful information about the internal conversion process from this measurement, a comparison with the theoretical calculations must be made. However, as pointed out earlier in Chapter II, interpolation errors in the tables of R and SB may be quite large for the L-subshell internal conversion coefficients for low-energy E2 transitions. Errors of this type may be partially eliminated by a careful interpolation procedure.

In this investigation, a sophisticated interpolation procedure devised by Dingus and Rud was used to obtain the L-subshell internal conversion coefficients[1]. The actual computer calculations were performed by Dingus at the University of Colorado. The procedure was to use the method discussed by Hildebrand in which a search was made for a minimum error term using "Newton's interpolation formula with divided differences" (51). The error term converged to a minimum when the correct number of data points were considered. None of the interpolated internal conversion coefficients in the tables of R and SB were used in this calculation; instead only the calculated coefficients were considered (For example, in R, the internal conversion coefficients at Z = 35, 45,..., 95 were used).

Using the above method, an interpolation, performed first on atomic number (Z) and then on energy (k), was followed by an interpolation performed first on k and then on Z. The results of these two types of interpolations were consistent and the final theoretical L-subshell internal

---

[1] Dingus, R. S., Boulder, Colorado. Comparison of theoretical conversion coefficients. Private communication. 1967.

conversion coefficients were taken as the average of these two interpolations. In this manner interpolated values were obtained from the calculations in R and from those in SB for each of the three L-subshells.

The theoretical total internal conversion coefficient was calculated from the theoretical L-shell internal conversion coefficient and a knowledge of the ratio, $\alpha_L/(1+\alpha)$, obtained from beta-ray spectrometer measurements. Unfortunately, this ratio has not been measured for the 45-keV transition in U-236; however, for similar E2 transitions in Ra-226, Th-228, U-234, and Pu-240, $\alpha_L/(1+\alpha)$ has been measured to be 0.701 ± 0.014, 0.731 ± 0.007, 0.764 ± 0.007, and 0.710 ± 0.007, respectively (38). An average value of 0.73 ± 0.03 was used for $\alpha_L/(1+\alpha)$ for the E2 transition in U-236.

The various interpolated internal conversion coefficients are listed along with the experimental internal conversion coefficient in Table 3. The uncertainty shown in the theoretical values results from the uncertainty in $\alpha_L/(1+\alpha)$. As can be seen, the agreement with the theoretical result is quite good and, apparently , there is no significant deviation in the total internal conversion coefficient between experiment and theory for this transition.

Table 3. Total internal conversion coefficient for the 45-keV transition in U-236

	α_{L_I}	$\alpha_{L_{II}}$	$\alpha_{L_{III}}$	α_L	α
Calc. in R	11	239	214	464	635 ± 26
Calc. in SB	8	239	210	457	626 ± 26
Present work	-	-	-	-	607 ± 29

It should be pointed out that α_{L_I} is at least a factor of 20 less than $\alpha_{L_{II}}$ and $\alpha_{L_{III}}$. Thus, a very large deviation in α_{L_I} does not affect α to a noticable extent. In order to determine α_{L_I}, the L-subshell ratios must be measured. Several measurements of this type have been performed for low-energy E2 transitions in Pu-240 and Th-228 (52). Both the cases $\alpha_{L_I}/\alpha_{L_{II}}$ and $\alpha_{L_I}/\alpha_{L_{III}}$ were found to be in excellent agreement with SB. The agreement with R was not as good, possibly because of interpolation errors in the tables. Therefore, while the L-subshell ratios have not been measured for this transition in U-236, α_{L_I} is not expected to differ by more than a few percent from the tabulated values.

As mentioned in Chapter I, only a few previous measurements of total internal conversion coefficients have been made for low-energy E2 transitions in nuclei with A >226. These measurements, compiled by Stelson (37) using the Coulomb excitation results of Elbek (53) and Friedman et al. (54) and the lifetime measurements of Bell et al. (24), are presented in Table 4 along with the present result. The theoretical internal conversion coefficients are those listed by Stelson[1].

[1]For the U-236 transition it is interesting to note the difference between the theoretical value for α used in this investigation and the value quoted by Stelson (the tables of SB were used for both cases). Stelson did not indicate his interpolation procedure.

Table 4. Total internal conversion coefficients for E2 transitions

Nucleus	Energy (keV)	α, exp.	α, theory[a]	$\frac{\alpha, \text{ exp.}}{\alpha, \text{ theory}}$
Th-232	50±1	260±30	307	0.85±0.12
U-238	44.7	558±60	625	0.89±0.11
U-234	43.5	702±80	717	0.98±0.11
U-236	45.28	575±120	586	0.98±0.21
Pu-240	42.9	868±78	897	0.97±0.09
Present Work				
U-236	45.28	607±29	626±26	0.97±0.06

[a]The α, theory used here are by Sliv and Band. No errors are assigned except for the value interpolated in the present work.

All of the listed experimental conversion coefficients are less than the corresponding theoretical values; however, with the large uncertainties in the Coulomb excitation results, this trend should not be considered meaningful until further experimental results are available. In particular, for the 45-keV transition in U-236, both experimental internal conversion coefficients are in agreement with either of the two theoretical values listed for this transition.

VII. CONCLUSION

The most important result of this investigation is that, for the case studied, no internal conversion anomaly has been observed corresponding to those reported for several E2 transitions in the deformed nuclei centered in the rare-earth region. This investigation supports the view that any large anomalies in the total internal conversion coefficients for E2 transitions result from hidden experimental errors or numerical mistakes in the theoretical calculations.

As discussed in Chapter VI, the results of this investigation are essentially insensitive to the value of α_{L_I}; thus, nothing can be said about the experimental agreement in the L_I-subshell. On the other hand, it can be concluded definitely that there are no large deviations in $\alpha_{L_{II}}$ and $\alpha_{L_{III}}$ introduced by screening effects or nuclear deformation effects.

As experimental accuracies improve, accurate calculations of internal conversion coefficients for higher electron shells will need to be performed. M-, N-, and O-subshell internal conversion coefficients for E2 transitions have already been measured (55), and the actual environment of the atom may affect these higher-shell conversion coefficients.

Finally, it must be emphasized that since the above results apply to the U-236 transition only, other measurements of this type should be performed to see if these conclusions are valid for E2 transitions over the entire deformed nuclei region of A >226. For example, using the coincidence method, a measurement of the total internal conversion coefficient of the 57-keV E2 transition in Th-228 can be made with an expected uncertainty of about three percent. Internal conversion coefficient measurements of transitions such as this one will be performed as sources become available.

VIII. APPENDIX: THE ELIMINATION OF PULSE PILE-UP

In any experiment employing the pulse height analysis of random events, the pulse height information may be distorted because of the random summing of pulses. This effect is called pile-up. For uncorrelated pulses the total number of distorted pulses, n, due to pile-up effects is

$$n = N(1 - e^{-at}) \tag{16}$$

where N is the total number of pulses, a is the mean counting rate, and t is the time during which random summing is important (42). When at is much less than unity,

$$n \cong N(at). \tag{17}$$

A plot of the percent of disturbed pulses as a function of count rate for various values of the pile-up time, t, is shown in Fig. 11.

For the particular case of nuclear spectroscopy, pulse pile-up occurs if the mean time between pulses is comparable to the recovery time of the electronic system. Because of pile-up, intensity determinations or even line recognition may be difficult. For example, a weak high-energy line may not be seen because of the random summing of intense low-energy pulses. In the following sections, the nature of pile-up will be discussed, and a method for rejecting pulses distorted by pile-up will be presented.

A. The Nature of Pile-up

When an event is detected by a nuclear detector such as a NaI(Tl) detector, a charge pulse is produced which is integrated in the preamplifier, creating a voltage pulse characterized by an abrupt rise followed by an exponential decay. At normal count rates and with a decay time constant of one millisecond, very few of the pulses will fail to overlap. Thus, at

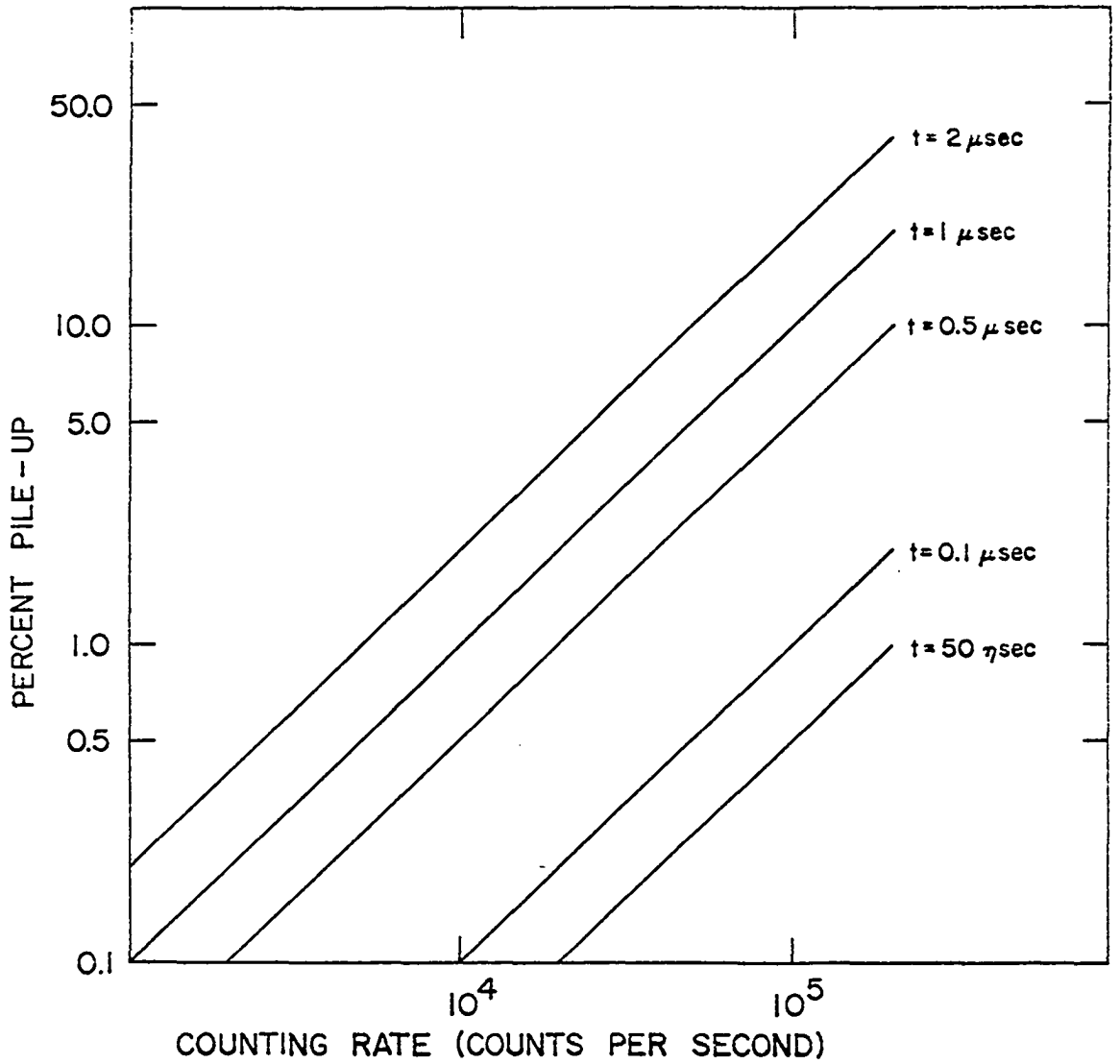

Fig. 11. Pulse pile-up as a function of counting rate and pile-up time

high count rates, the instantaneous base line in the preamplifier can fluctuate and can drive the output stage over a wide dynamic range. If there is any nonlinearity in this stage, pulses at the extremes of the range have distorted heights with a resulting effect on the pulse height distribution. This type of pile-up can occur at all signal points up to the first differentiator in the main amplifier (56).

Since the first differentiator shortens the pulse to about one microsecond, pile-up in the main amplifier can occur only on the primary pulse (random summing of the information carrying portions of two pulses) or on the undershoots of these pulses (random summing of a primary pulse with the undershoot of a preceding pulse). Pile-up on the primary pulse results in a distorted pulse shape with a pulse height which is higher than normal. As was shown in Fig. 11, the probability of this type of pile-up is strongly dependent on count rate. At high count rates, pulse shaping in the main amplifier is normally accomplished by the use of either double RC differentiation or double delay-line clipping. Since these pulse-shaping techniques result in a bipolar pulse with shortened undershoot, the amplifier recovery time is greatly reduced, and pile-up on the undershoot is essentially eliminated (56). There is not way to eliminate pile-up on the primary pulses without special circuitry.

B. The Elimination of Primary Pulse Pile-Up

Two basic methods are used to eliminate primary pulse pile-up. First the timing between pulses can be examined before the main amplifier, and subsequent circuits can be gated off (for example, the linear gate at the input of a multichannel analyzer) whenever two or more pulses occur within

a preset time. Several circuits using this idea have been designed (57-60). The second method is to examine the pulse shape at the output of the main amplifier and to gate off subsequent circuits whenever distorted pulses are detected. The first method is advantageous because pile-up in the preamplifier can be partially eliminated; however, more sophisticated electronics are usually necessary than in the second method. For the present experiment, the second method was particularly easy to apply because of the unique shape of a pile-up pulse at the output of a double delay-line amplifier.

In a double delay-line amplifier (DD2) the input pulse, idealized as a step function, is delayed a time τ and inverted. This delayed pulse is added to the original pulse resulting in a square pulse of width τ. The process is then repeated using the square pulse generated with the first delay-line clip, creating a bipolar symmetric output pulse of total width 2τ. Therefore, as can be seen in the first three pulse diagrams in Fig. 12, for two input pulses separated in time by an amount Δ which is less than τ, the time difference between the leading edge of the positive part and the leading edge of the negative part of the DD2 output pulse (after the second delay-line clip) will be $\tau+\Delta$. For this reason, one method of eliminating primary pulse pile-up is to gate off subsequent circuits whenever this time differences exceeds τ. Several circuits using this method have been constructed (61-63). For the present experiment a relatively simple circuit was built using this method.

The basic philosophy of the present design is that if two identical square pulses, one delayed with respect to the other by an amount τ, are fed into a coincidence circuit, an output signal will be produced whenever the input pulse width exceeds τ. The coincidence output can then be used as a pile-up detection signal. The main elements of this circuit, shown in Fig.

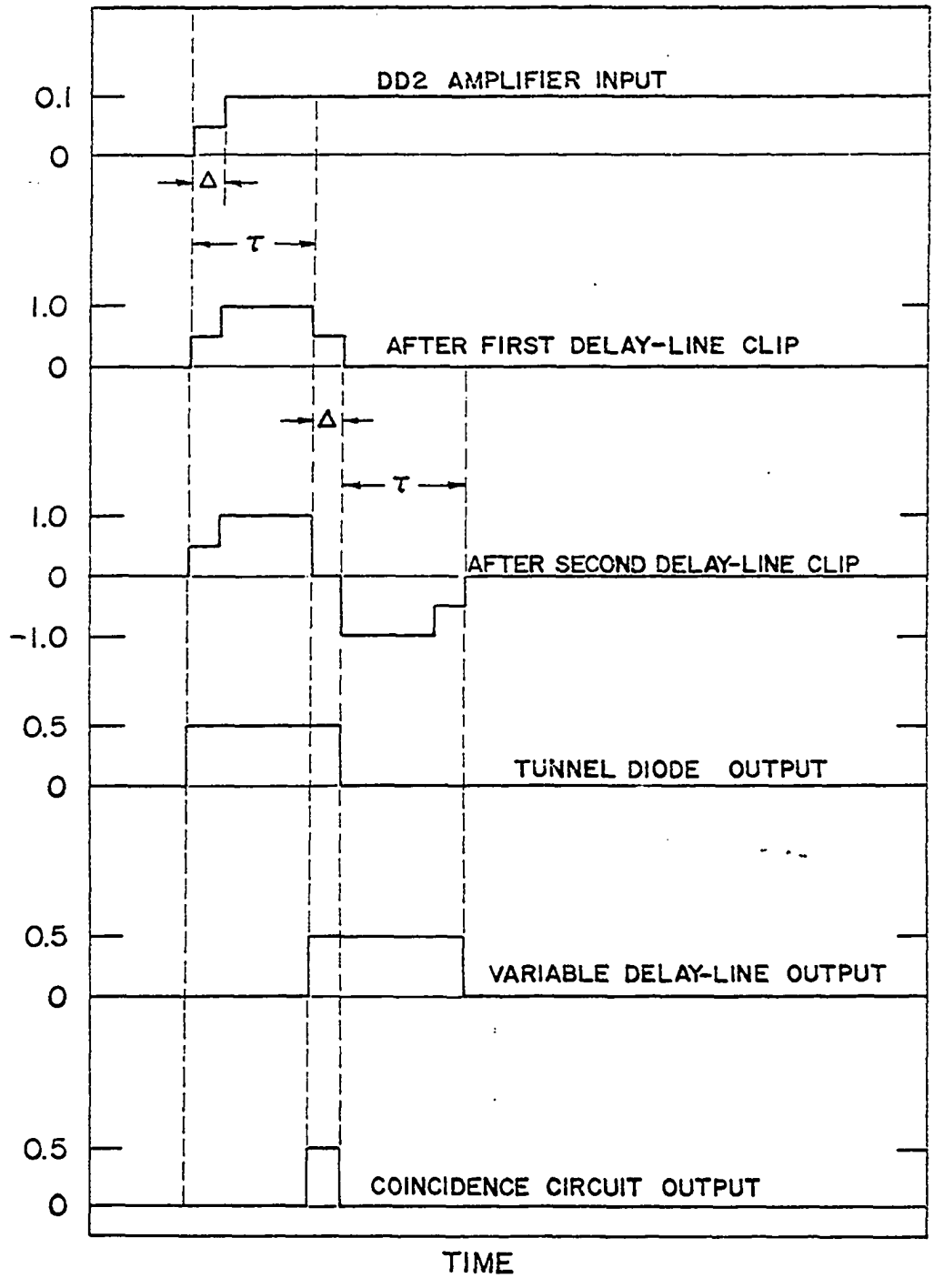

Fig. 12. Pulse shapes in electronic system during pile-up

13, are a pulse-shaping network followed by a variable delay line and a Garwin coincidence unit (64). The pulse-shaping network is composed of a non-overloading amplifier with a variable gain of one through ten followed by a tunnel diode bistable multivibrator. The non-overloading amplifier amplifies the pulse from the DD2 amplifier, insuring triggering of the tunnel diode at the 20-mV level of the input pulse. The tunnel diode circuit produces a fast-rise 0.5-V pulse which has a width equal to the time difference between the leading edges of the positive and negative portions of the DD2 output pulse. Thus, the pulse-shaping network converts the relatively slow-rising pulse from the DD2 amplifier to a fast-rising square pulse whose width can be accurately determined. The width of this pulse is then measured by the coincidence circuit after the input to one leg has been delayed an amount selected by the variable delay line. The pulse shape at various points in the DD2 amplifier and pile-up rejection circuit are shown in Fig. 12, and a schematic diagram of the pile-up rejection circuit is shown in Fig. 14.

The performance of this pulse-width detector was quite satisfactory. By introducing pulses with a fast risetime into the DD2 amplifier from two precision pulse generators, one triggered by the other after a variable time delay, a piled-up pulse could be artificially created. Thus, the pile-up resolution (defined as the minimum separation of two pulses that could be detected by this circuit) could be accurately measured. For an input pulse of constant amplitude this resolving time could be made as small as 10 nsec by careful adjustment of the variable delay line. However, the pulse width for a non-overlapping pulse at the output of the tunnel diode multivibrator depended somewhat on the DD2 output pulse height. The same variable delay-

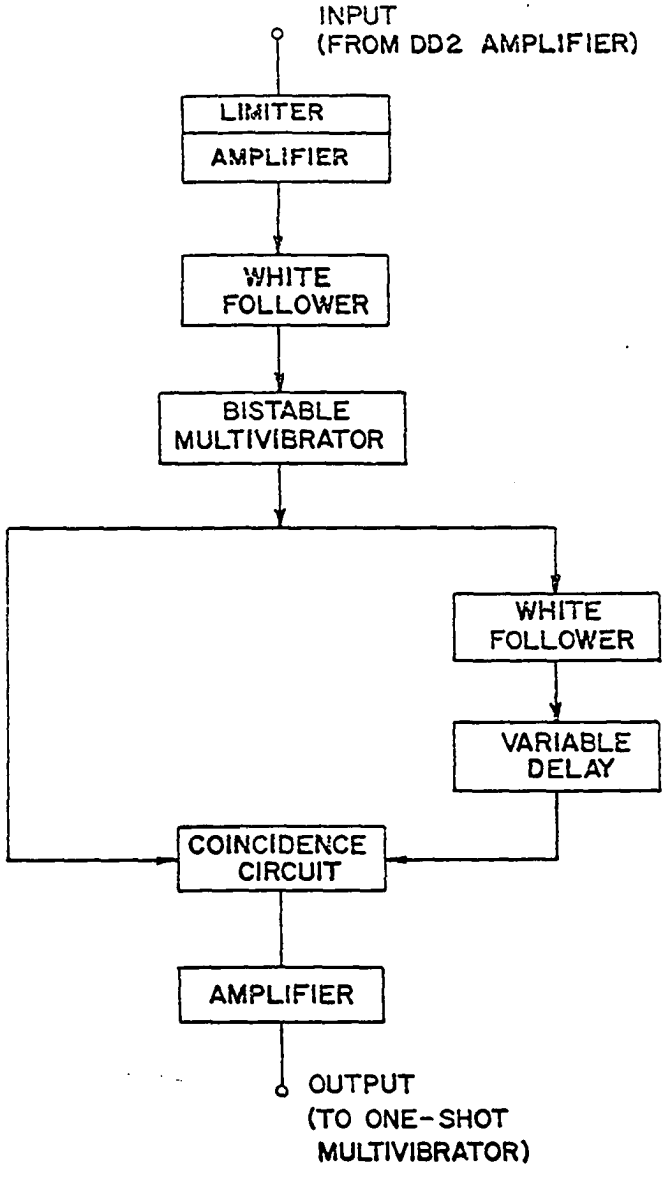

Fig. 13. Block diagram of the pile-up rejection circuit

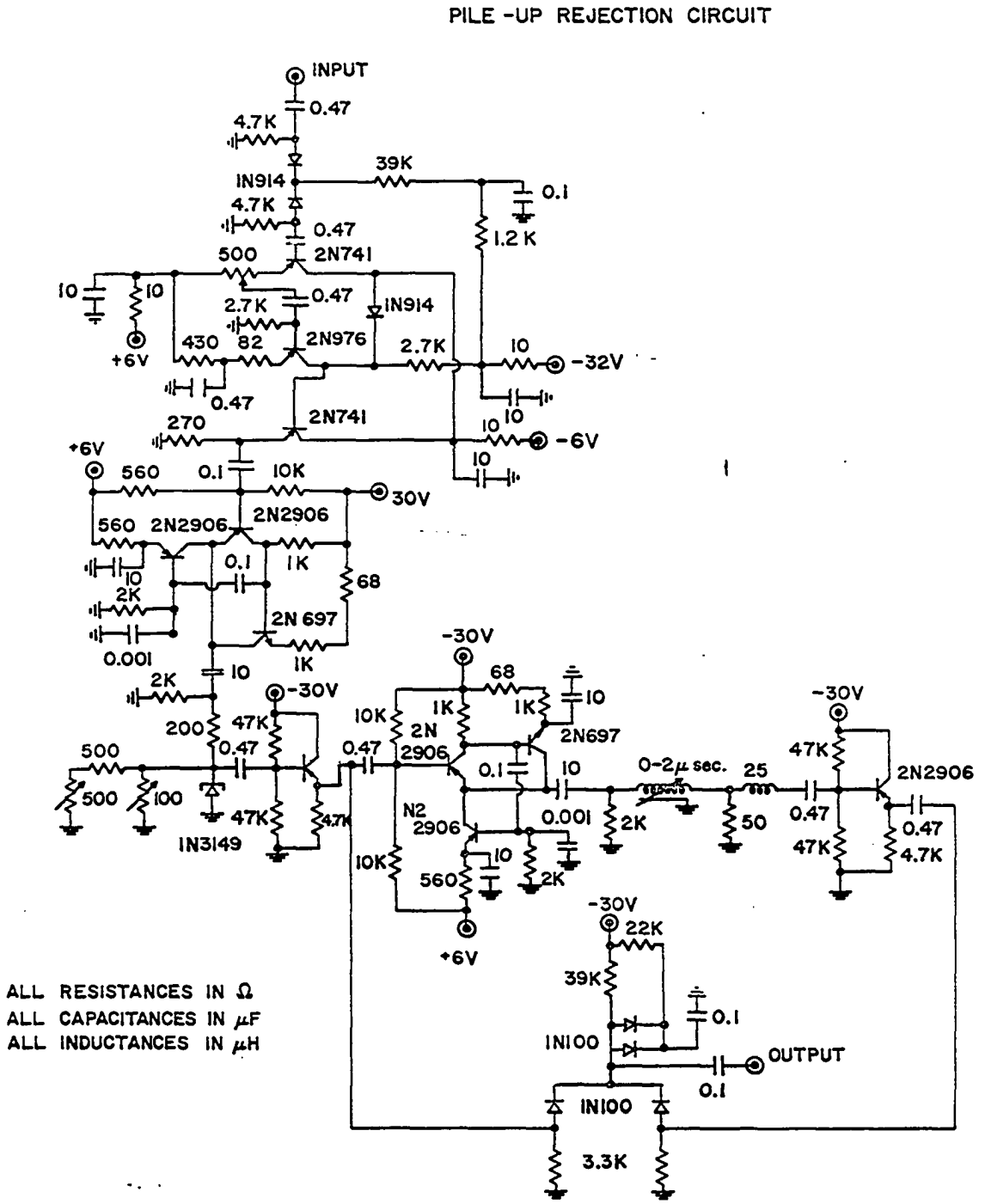

Fig. 14. Schematic diagram of the pile-up rejection circuit

line setting that gave a 10-nsec resolving time for a 1-V DD2 output pulse. This effect was much more noticable if the DD2 input pulse had a slow risetime. For example, when the pulse generator risetime was adjusted to 0.5 μsec, the resolving time for a 1-V DD2 output pulse increased from 20 nsec to 40 nsec for an initial 10-nsec resolving time at 10 V. This increase was expected because an increase in the risetime implied a decrease in the accuracy with which the initial time of the leading edge of the pulse could be measured.

This circuit can be used to eliminate a large fraction of primary pulse pile-up. Two added advantages are; overload pulses are detected since the width of a DD2 amplifier output pulse increases as the amplifier goes into saturation, and pile-up of a primary pulse on the negative part of a preceeding DD2 amplifier output pulse is detected. Perhaps the major disadvantage of this circuit is that the pile-up resolution is not equal for all regions of the pulse height distribution; in fact, this circuit cannot be used when constant pile-up resolution is needed for more than one region of a complex spectrum. On the other hand, if the spectrum has only one high-intensity photon group as in this investigation, this type of pile-up rejection is entirely adequate.

C. Reduction of Pile-up Effects in a NaI(Tl) Pulse Height Spectrum

One of the most important applications of the pile-up detector described in the previous section is the reduction of pile-up effects at high count rates in NaI(Tl) spectra. For this application the output of the pile-up detector was used to trigger a one-shot multivibrator which generated a pulse suitable for closing the gate at the input of a multichannel analyzer. Several Cs-137 spectra were taken, some with pile-up rejection and some

without pile-up rejection.

Since Cs-137 has only a single gamma ray at 662 keV, the main effect of pile-up at high count rates is to introduce an asymmetrical random sum peak at an energy of 2 x 662 keV with the low-energy side extending down to 662 keV (65). This peak is created by the random summing of pulses from 662-keV gamma rays with other pulses in the pulse height distribution. For example, a Gaussian sum peak at 2 x 662 keV is created when pulses from two 662-keV gamma rays exactly overlap. The distribution below this sum peak is the result of both the partial overlapping of two 662-keV pulses and the summing of a 662-keV pulse with a pulse corresponding to a lower energy in the pulse height distribution.

As can be seen in Fig. 15, the random sum peak was drastically reduced when pile-up rejection was included. By taking the ratio of the number of counts in the 2 x 662-keV peak to the number of counts in the 662-keV photopeak, the pile-up resolving time was calculated from Equation 17 to be 30 nsec. However, since the pulse width as measured by the pile-up rejection circuit is a function of pulse height, a better method to estimate an average pile-up resolving time is to compare the number of counts above the 662-keV photopeak with pile-up rejection included to the number of counts above the photopeak without pile-up rejection included. The pile-up resolving time obtained with this method was 50 nsec , which was comparable to the resolving times obtained from other reported pile-up rejection circuits (58-64).

In summary, if the preamplifier is not driven to the extremes of its range so that pile-up in the preamplifier does not result in preamplifier distortion and if the above circuit is used to eliminate primary pulse

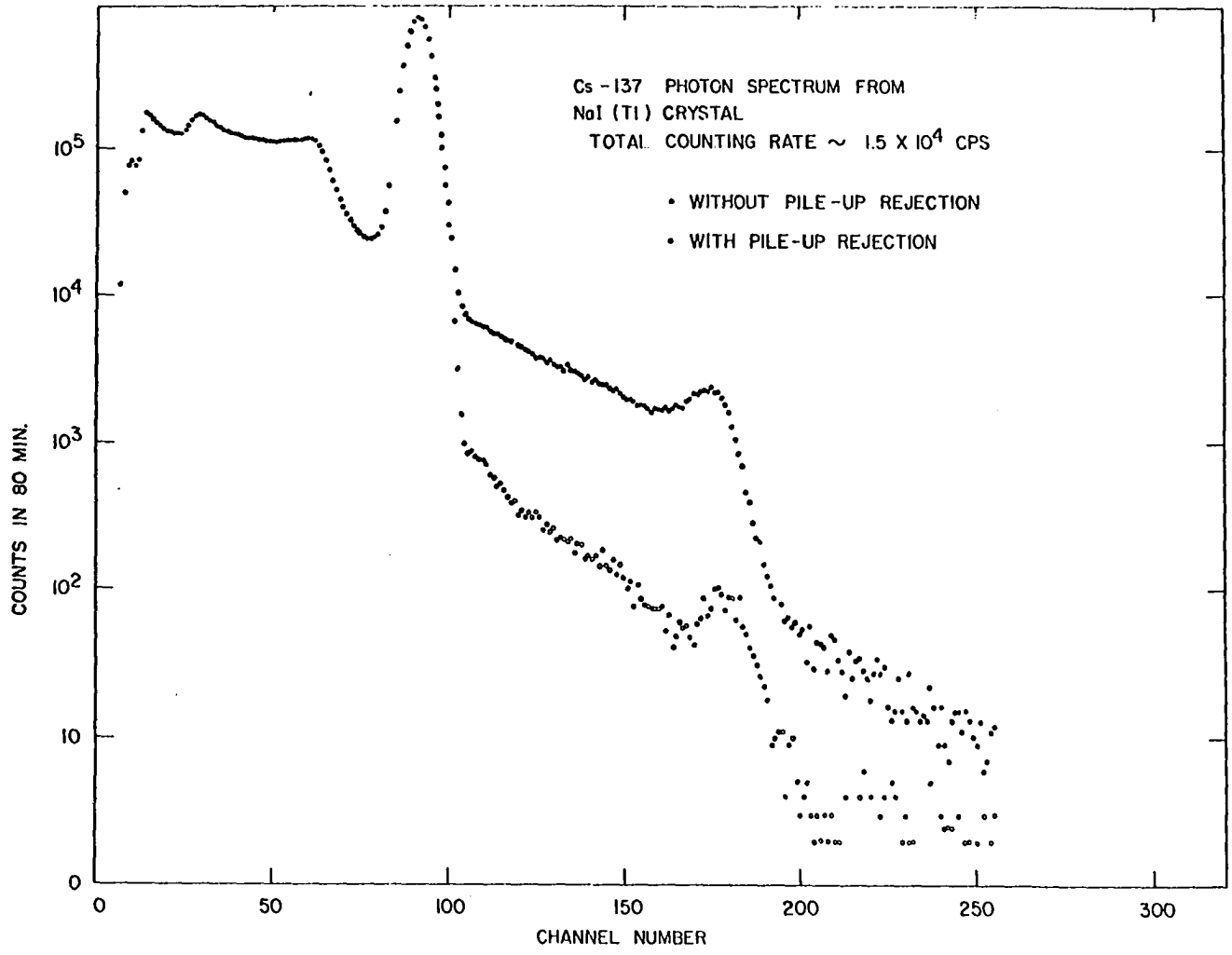

Fig. 15. Comparison of Cs-137 spectra with and without pile-up rejection

pile-up, the effect of pile-up can be reduced by about a factor of 25 for the case of simple NaI(Tl) spectra. In the present experiment, count rates were of the order of 1000 counts per second and with this circuit, primary pulse pile-up was reduced from 0.1 percent to 0.004 percent.

IX. LITERATURE CITED

1. van Baeyer, O. and Hahn, O., Magnetische Linienspektren von β-Strahlen, Physik. Z. 11, 488 (1910).

2. Meitner, L., Die γ-Strahlung der Actinumreihe und der Nachweis, dass die γ-Strahlen erst nach erfolgtem Atomzerfall emittiert werden, Z. Physik 34, 807 (1925).

3. Ellis, C.D. and Wooster, W.A., The heating effect of the γ-rays of radium B and radium C, Lond. Edin. and Dublin Phil. Mag., Ser. 6 50, 521 (1925).

4. Hulme, H.R., The internal conversion coefficient for radium C, Proc. Roy. Soc. (London), Ser. A 138, 643 (1932).

5. Taylor, H.M. and Mott, N.F., A theory of the internal conversion of γ-rays, Proc. Roy. Soc. (London), Ser. A 138, 665 (1932).

6. Fisk, J.B. and Taylor, H.M., The internal conversion of γ-rays, Proc. Roy. Soc. (London), Ser. A 146, 178 (1934).

7. Taylor, H.M. and Mott, N.F., The internal conversion of γ-rays; II, Proc. Roy. Soc. (London), Ser. A. 142, 215 (1933).

8. von Weizsäcker, C. F., Metastabile Zustände der Atomkerne, Naturwissenshaften 24, 813 (1936).

9. Hebb, M. H. and Uhlenbeck, G. E., Stability of nuclear isomers, Physica 5, 605 (1938).

10. Dancoff, S. M. and Morrison, P., The calculation of internal conversion coefficients, Phys. Rev. 55, 122 (1939).

11. Drell, S. D., The magnetic internal conversion coefficient, Phys. Rev. 75, 132 (1949).

12. Rose, M. E., Goertzel, G. H., Spinrad, B. I., Harr, J., and Strong, P., The internal conversion coefficients. I: the K-shell, Phys. Rev. 83, 79 (1951).

13. Rose, M. E., Theory of internal conversion, in Siegbahn, K., ed., Beta- and gamma-ray spectroscopy, pp. 396-413, 905-909, Interscience Publishers, Inc., New York, N. Y. (1955).

14. Sliv, L. A., Calculation of final state of nuclei from calculation of coefficient of internal conversion (Translated title), Zhur. Eksp. i teoret. fiz. 21, 770 (1951). Original available but not translated; abstracted in Nuclear Science Abstracts, No. 3 6, 134 (1952).

15. Sliv, L. A. and Band, I. M., Tables of internal conversion coefficients, in Siegbahn, K., ed., Alpha-, beta-, and gamma-ray spectroscopy Vol. 2, pp. 1639–1672, North-Holland Publishing Co., Amsterdam (1965).

16. Wapstra, A. H. and Nijgh, G. J., Indications for a strong influence of the nuclear size on magnetic dipole conversion coefficients, Nuclear Phys. 1, 245 (1956).

17. Rose, M. E., Internal conversion coefficients, Interscience Publishers, Inc., New York, N. Y. (1958).

18. Church, E. L. and Weneser, J., Effect of the finite nuclear size on internal conversion, Phys. Rev. 104, 1382 (1956).

19. Gurney, R. W., The number of particles in the beta-ray spectrum of radium B and radium C, Proc. Roy. Soc. (London), Ser. A 109, 540 (1925).

20. McGowan, F. K. and Stelson, P. H., Internal conversion coefficients for pure E2 and mixed E2 + M1 transitions, Phys. Rev. 107, 1674 (1957).

21. Subba Rao, B. N., Internal conversion coefficients of E2 transitions, Nuovo cimento 17, 189 (1960).

22. Bernstein, E. M., Anomalous E2 internal conversion coefficients for rotational transitions, Phys. Rev. Letters 8, 100 (1962).

23. Brahmavar, S. M. and Ramaswamy, M. K., Anomalies in internal conversion coefficients of E2 transitions in even-even nuclei, in Hamilton, J. H., ed., Internal conversion processes, pp. 225-235, Academic Press, Inc., New York, N. Y. (1966).

24. Bell, R. E., Bjornholm, S., and Severiens, J. C., Half lives of first excited states of even nuclei of Em, Ra, Th, U, and Pu, Mat. Fys. Medd. Dan. Vid. Selsk., No. 12 32, 1 (1960).

25. Rose, M. E., Internal conversion theory, in Hamilton, J. H., ed., Internal conversion processes, pp. 15-33, Academic Press, Inc., New York, N. Y. (1966).

26. Rose, M. E., Multipole fields, John Wiley and Sons, Inc., New York, N. Y. (1955).

27. Church, E. L. and Weneser, J., Nuclear structure effects in internal conversion, Ann. Rev. Nuclear Sci. 10, 193 (1960).

28. Green, T. A. and Rose, M. E., Nuclear structure effects in internal conversion, Phys. Rev. 110, 105 (1958).

29. Kramer, G. and Nilsson, S. G., The penetration effect in electric dipole internal conversion, Nuclear Phys. 35, 273 (1962).

30. Nilsson, S. G. and Rasmussen, J. O., On anomalous conversion coefficients of dipole transitions, Nuclear Phys. 5, 617 (1958).

31. Listengarten, M. A., Internal conversion: a review, Bull. Acad. Sci. USSR, Phys. Ser. 22, 755 (1958).

32. Dingus, R. S. and Rud, N., Comparison of theoretical conversion coefficients, (Abstract), Bull. Am. Phy. Soc. 12, 67 (1967).

33. Bhalla, C. P., Internal conversion coefficients for magnetic multipoles for Z = 39, Z. Physik 196, 26 (1966).

34. Bhalla, C. P., Internal conversion coefficients with relativistic Hartree-Fock model for the deformed region, Phys. Rev. 157, 1136 (1967).

35. Hultberg, S. and Stockendal, R., On the determination of absolute internal conversion coefficients by the comparison of conversion lines and photolines, Arkiv Fysik 14, 565 (1959).

36. Easterday, H. T., Haverfield, A. J., and Hollander, J. M., An internal conversion coefficient spectrometer utilizing semi-conductor detectors, Nucl. Instr. Methods 32, 333 (1965).

37. Stelson, P. H., Information on conversion coefficients from Coulomb excitation and lifetime measurements, in Hamilton, J. H., ed., Internal conversion processes, pp. 213-223, Academic Press, Inc., New York, N. Y. (1966).

38. Engelkemeir, D. and Halley, J., L fluorescence yields in heavy elements, Phys. Rev. 134, 24 (1964).

39. Dingus, R. S., Talbert, W. L., and Stewart, M. G., Measurements of conversion coefficients for transitions in Gd^{154}, Dy^{160}, Yb^{171}, and Pr^{141}, Nuclear Phys. 83, 545 (1966).

40. Dingus, R. S., Talbert, W. L., and Hatch, E. N., Measurements of some internal conversion coefficients using scintillation counter techniques, U. S. Atomic Energy Commission Report IS-1032 (Iowa State Univ., Ames. Inst. for Atomic Research), (1965).

41. Hyde, E. K., Perlman, I., and Seaborg, G. T., The nuclear properties of the heavy elements: II. Detailed radioactive properties, Prentice-Hall Inc., Englewood Cliffs, N. J. (1964).

42. Evans, R. D., The atomic nucleus, McGraw-Hill Book Co., New York, N. Y. (1955).

43. Chetham-Strode, A., Tarrant, J. R., and Silva, R. J., The application of silicon detectors to alpha particle spectroscopy, IRE Transactions on Nuclear Sci., No. 1, NS-8, 59 (1961).

44. Frauenfelder, H. and Steffen, R. M., Angular correlations, in Siegbahn, K., ed., Alpha-, beta- and gamma-ray spectroscopy Vol. 2, pp. 997-1198, North-Holland Publishing Co., Amsterdam, (1965).

45. Murphy, E. S., Alpha-gamma angular correlation measurements with liquid sources, U. S. Atomic Energy Commission Report ANL-6685 (Argonne National Laboratory), (1963).

46. Milton, J. C. D., and Fraser, J. S., The α-γ angular correlation in the decay of Ra^{224}, Ra^{226}, and Pu^{238}, Phys. Rev. 95, 628 (1954).

47. Valladas, G., Teillac, J., Falk-Vairant, P., and Benoist, P., Correlations angulaires α-γ et α-rayonnement X dans lo (Th^{230}), J. Phys. Radium 16, 125 (1955).

48. Grodstein, G. W., X-ray attenuation coefficients from 10 keV to 100 MeV, National Bureau of Standards Circular NBS 583 (1957).

49. McGowan, F. K., Measure of K-shell internal conversion coefficients with a coincidence scintillation spectrometer, Phys. Rev. 93, 163 (1954).

50. Eldridge, J. S. and Crowther, P., Absolute determination of I^{125} in clinical applications, Nucleonics, No. 6 22, 56 (1964).

51. Hildebrand, F. B., Introduction to numerical analysis, McGraw-Hill Book Co., Inc., New York, N. Y. (1956).

52. Hamilton, J. H., van Nooijen, B., Ramayya, A. V., and Brantley, W. H., L subshell ratios for E2 transitions in deformed heavy elements, in Hamilton, J. H., ed., Internal conversion processes, pp. 541-547, Academic Press, Inc., New York, N. Y. (1966).

53. Elbek, B., Determination of nuclear transition probabilities by Coulomb excitation, Munksgaards, Copenhagen (1963). Original not available; cited in Hamilton, J. H., ed., Internal conversion processes, p. 219, Academic Press, Inc., New York, N. Y. (1966).

54. Friedman, A. M., Erskine, J. R., and Braid, T. H., Measurement of the quadrupole moments and deformation of Th^{230}, U^{234}, U^{236}, Pu^{240}, and Pu^{242} by inelastic scattering of deuterons, (Abstract), Bull. Am. Phys. Soc. 10, 540 (1965).

55. Amtey, S. R., Hamilton, J. H., Ramayya, A. V., and van Nooijen, B., M, N, and O subshell conversion coefficients in Th^{228} and Pu^{240}, Phys. Rev. 149, 922 (1966).

56. Fairstein, E. and Hahn, J., Nuclear pulse amplifiers- fundamentals and design practice, Nucleonics, No. 9 23, 81 (1965).

57. Bengston, B., Jastrzebski, J., and Moszynski, M., Reduction of pile-up effects in time and energy measurements, Nucl. Instr. Methods 47, 61 (1967).

58. Weisberg, S., A pile-up elimination circuit, Nucl. Instr. Methods 32, 138 (1965).

59. McGervey, J. D. and Walters, V. F., Detection of pulse pile-ups with tunnel diodes, Nucl. Instr. Methods 25, 219 (1964).

60. Rosen, S., Pile-up rejection circuits, Nucl. Instr. Methods 11, 316 (1961).

61. Monier, L. F. and Tripard, G. E., Detection of pulse pile-ups with pulse overlap to pulse height convertor, Rev. Sci. Instr. 37, 316 (1966).

62. Fuschini, E., Maroni, C., and Veronesi, P., A circuit for rejecting piled-up pulses, Nucl. Instr. Methods 41, 153 (1966).

63. Segel, R. E., Reduction of pile-up contamination in pulse pile-up spectra; (abstract), Bull. Am. Phy. Soc. 7, 542 (1962).

64. Garwin, R. L., A fast coincidence-anticoincidence analyzer, Rev. Sci. Instr. 24, 618 (1953).

65. Bialkowski, J., Jasińske, A., and Ludziejewski, J., Shape of the random sum photo-peak in scintillation spectrometry, Nucl. Instr. Methods 31, 90 (1964).

X. ACKNOWLEDGMENTS

The writer wishes to express his gratitude to the following people who have helped make this investigation a success:

Dr. R. S. Dingus who initially suggested this investigation, devised the experimental technique, and performed the computer interpolations.

Mr. L. Mourlam of the Instrumentation Group for helpful suggestions in the design of the pile-up rejection circuit.

Mr. C. Weber of the Reactor Division Electronics Group for invaluable help in maintaining the multichannel analyzer.

Various people of the Computer Services Group for their aid in the computations.

Mr. J. Lerner for making the Pu-240 sources at the Argonne National Laboratory.

The National Aeronautics and Space Administration for providing financial assistance during the latter part of his graduate training.

Above all the author wishes to thank Dr. W. L. Talbert for skillfully guiding this investigation from its inception.